Multi-step Rhodopsin Inactivation Schemes Can Account for the Size Variability of Single Photon Responses in *Limulus* Ventral Photoreceptors

MARC A. GOLDRING and JOHN E. LISMAN

From the Department of Biology and Center for Complex Systems, Brandeis University, Waltham, Massachusetts 02254

ABSTRACT *Limulus* ventral photoreceptors generate highly variable responses to the absorption of single photons. We have obtained data on the size distribution of these responses, derived the distribution predicted from simple transduction cascade models and compared the theory and data. In the simplest of models, the active state of the visual pigment (defined by its ability to activate G protein) is turned off in a single reaction. The output of such a cascade is predicted to be highly variable, largely because of stochastic variation in the number of G proteins activated. The exact distribution predicted is exponential, but we find that an exponential does not adequately account for the data. The data agree much better with the predictions of a cascade model in which the active state of the visual pigment is turned off by a multi-step process.

INTRODUCTION

Signal transduction commonly involves an enzyme cascade in which the activation of a single receptor molecule triggers a sequence of gain-producing reactions (Stadtman and Chock, 1979). For instance, in vertebrate rod photoreceptors a light-activated rhodopsin molecule works as an enzyme to activate hundreds of G proteins. Each of these activates a cGMP phosphodiesterase enzyme that hydrolyzes many molecules of cGMP. This second messenger, in turn, controls the channels that gate the flow of ions through the membrane (reviewed in Stryer, 1986). In such a cascade, each molecule will have a randomly variable active lifetime, in analogy with a channel protein, which has a randomly variable open time (Colquhoun and Hawkes, 1984). Therefore, the gain produced by each molecule will be stochastic in nature. Stochastic gain at the molecular level implies that the output of the cascade (e.g., the flow of ions) will vary randomly. Such variability may go unnoticed in laboratory experiments

Address correspondence to John E. Lisman, Department of Biology and Center for Complex Systems, Brandeis University, Waltham, MA 02254.

Dr. Goldring's present address is HO 2N-409, AT&T Bell Laboratories, 101 Crawfords Corner Road, P.O. Box 3030, Holmdel, NJ 07733-3030.

J. GEN. PHYSIOL. © The Rockefeller University Press · 0022-1295/94/04/0691/37 $2.00
Volume 103 April 1994 691–727

because typically, many receptor molecules are activated by a stimulus and the fluctuations in their respective outputs tend to cancel. Photoreceptors, however, provide a system in which the stochastic response to a single activated receptor molecule can be studied. This is particularly true in *Limulus* photoreceptors, where the photoexcitation of a single rhodopsin molecule stimulates a large discrete wave of membrane depolarization (quantum bump; Fuortes and Yeandle, 1964; Lillywhite, 1977). Voltage (Millecchia and Mauro, 1969) and patch (Bacigalupo, Chinn, and Lisman, 1986) clamp studies of the ventral photoreceptor have shown that a quantum bump results from inward current through thousands of transiently open membrane channels. Thus, a quantum bump is a direct manifestation of the large amplification produced by the transduction cascade (Cone, 1973). Strikingly, quantum bumps are highly variable in size (Yeandle and Spiegler, 1973), latency (Martinez and Srebro, 1976) and waveform shape (Goldring, 1980; Stieve, Reuss, Hennig, and Klomfass, 1990). A question that naturally arises is why this variability occurs and whether it can be explained in terms of the properties of the transduction cascade.

Borsellino and Fuortes (1968) explored the implications of quantum bump latency variability. They worked with a stochastic version of the original, deterministic cascade model that Fuortes and Hodgkin (1964) had earlier shown to be consistent with the response to a moderately bright flash (which reflects average quantum bump kinetics). Studies subsequent to that of Borsellino and Fuortes, however, revealed analytical difficulties in interpreting latency variability when even the simplest cascade models are invoked (Tiedge, 1981; Goldring and Lisman, 1983). In this paper, we demonstrate that the size of the quantum bump, quantified as the time-integral of quantum bump current (charge), can be more easily related to cascade properties. We find that for simple models, a high size variability is expected, largely because of a high variability in the number of G proteins activated by rhodopsin. In particular, we show that for the simplest models–those in which rhodopsin and all other active molecules are inactivated in a single step–the probability distribution for quantum bump charge has an exponential form, a conclusion also reached by Grzywacz and Hillman (1985). They examined measured quantum bump charge distributions and found good agreement with an exponential, in support of the simplest models. By contrast, we find that measured distributions are somewhat more peaked than an exponential. We go on to show that these distributions are consistent with simple models in which rhodopsin is turned off by a multi-step process. Direct experiments to test whether the shape of these distributions is dependent on early transduction processes involving rhodopsin are presented in the companion paper (Kirkwood and Lisman, 1994).

MATERIALS AND METHODS

Electrophysiological Recording and Data Acquisition

The ventral nerve of *Limulus* was continuously superfused with artificial sea water (ASW) of standard composition (in mM: 425 NaCl, 10 KCl, 10 $CaCl_2$, 22 $MgCl_2$, 26 $MgSO_4$, 15 Tris-Cl, pH 7.8). Substitution of 9 mM of the $CaCl_2$ in ASW with $MgCl_2$ yielded the 1-mM-Ca^{2+} sea

water used in one experiment in an effort to increase quantum bump size (Wong, 1977). The bath temperature, monitored with a thermocouple, was kept fixed to within 0.1°C.

To avoid recording from electrically coupled photoreceptors (Sokol and Srebro, 1982), only photoreceptors that appeared to be isolated were selected for study and the light stimulus was confined to a small ($\approx 10\mu$) spot. Photoreceptors were impaled with two microelectrodes (2.5 M KCl, 12–16 MΩ), voltage-clamped to resting potential (−45 to −60 mV) by standard methods (Lisman and Brown, 1971), allowed to dark-adapt about 1 hr (Lisman and Brown, 1975), cooled to 15.5–18°C to reduce the rate of spontaneous quantum bumps (Adolph, 1964; Srebro and Behbehani, 1972), and stimulated at regular intervals (1.3–2.5s) with a 3-ms flash of dim, 570-nm light that evoked ~0.3–1.3 quantum bumps on the average. If the quantum bump peak amplitude distribution (Yeandle and Spiegler, 1973), probability of response to a flash, spontaneous quantum bump arrival rate or resting current level (nominally 0 nA) were unstable, data were not taken. In most cases, however, these parameters became stable, at least by eye, at which point we recorded voltage clamp current through an RC filter (time constant 0.3 ms) and on f.m. magnetic tape (recorder model 3964A, Hewlett-Packard, San Francisco, CA; four-pole low-pass Butterworth response, cutoff frequency near 300 Hz). Data were taken until the cell deteriorated, as evidenced by a decrease in average quantum bump peak amplitude, a decrease in the probability of response and/or an increase in the arrival rate of

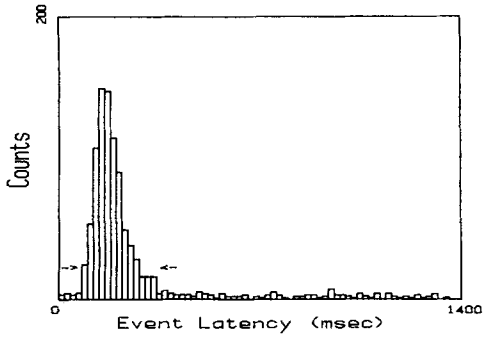

FIGURE 1. The event latency distribution for Cell 1. Bin width: 20 ms. See Materials and Methods for details.

spontaneous quantum bumps. After the experiment, recorded data were played out through a four-pole low-pass Butterworth filter set at a cutoff frequency of 150 Hz, digitized by a computer at 1000 Hz, and stored on disk.

The Measurement of Response Charge

The current trace following each flash was examined by eye using a computer and interactive graphics. Every event was measured, where an event consisted either of a single quantum bump or of multiple quantum bumps with temporally overlapping waveforms. To measure an event, two sections of baseline were chosen before and after the event, respectively, and a single line was fit through these sections by a linear least squares routine (Bevington, 1969, pp. 105–106). The charge of the event (in picoCoulombs, pC), was then measured as the integral of the event waveform above this line (unaffected by preliminary low-pass filtering), using an algorithm from Bevington (1969, pp. 272–275).

A latency distribution for events was compiled as in Fig. 1. This distribution consisted of a broad peak superposed on a low, uniform, background. The peak rose sharply from the background at small latencies and returned to the background level with a more gradual tail. The peak was due to light-induced quantum bumps, and these had a relatively restricted latency range, which is termed here the "response period"; the background was due to

spontaneous quantum bumps, which began at times uniformly distributed between flashes (Srebro and Yeandle, 1970). The response period was defined empirically as the latency range covered by all but the extreme upper tail of the peak (Fig. 1, *arrows;* see below). The observed response to a given flash was then taken to be all the events that began in the response period, and the "response charge" was computed as the sum of the charges of all these events. Because low flash strengths were used, a large number of flashes failed to yield any observed response (nonresponses) and were thus assigned a response charge of 0 pC.

The relative contributions of light-induced quantum bumps and spontaneous quantum bumps to observed responses were evaluated from the empirical probability of response (fraction of flashes followed by an observed response), p_{OBS}, and the rate of occurrence of spontaneous quantum bumps (see Table I and associated details in Appendix E). The rate of spontaneous quantum bumps was measured directly from the events beginning in a "spontaneous quantum bump observation period," which was chosen well outside the response period. The rate of events in the spontaneous quantum bump observation period was so low (< 0.13/s) that all these events could be regarded as single (i.e., nontemporally overlapping) spontaneous quantum bumps. We estimated that at least 90% of the observed responses comprised only light-induced quantum bumps (w_L, Table I). The few observed responses that contained spontaneous quantum bumps were incorporated into the response charge distribution analysis as described in Appendix A and below. We further estimated that a very small fraction (at most 3%) of the light-induced quantum bumps began outside the response period and were thus not included in observed responses. It is apparent from Appendix A that the omission of such quantum bumps is inconsequential if quantum bump size properties do not depend on latency. The independence of size and latency has been reported by previous workers (Howard, 1983; Stieve and Bruns, 1983) and is examined further in Results. In any case, because the quantum bumps at issue were so few in number, their systematic exclusion had no significant impact on our conclusions about distributions.

Despite the systematic exclusion from observed responses of the quantum bumps beginning after the response period, it was nevertheless theoretically possible for such quantum bumps to be included inadvertently in a response charge measurement. This could happen in the following way. An event beginning late in the response period would endure past the end of the response period, and then, before the event waveform had returned fully to the baseline, a new quantum bump would begin. Because the event would be integrated from its very beginning through its complete return to the baseline (see above), the new quantum bump would be included in the event, and hence, in tbe observed response. To verify that the number of such "contaminated" observed responses was acceptably small, we first considered the time interval t_{sep} by which two, consecutive quantum bumps would have to be separated in latency to be measured as separate events (e.g., see Fig. 2 F). We then estimated the fraction of flashes f for which quantum bumps began after the response period but within t_{sep} after the latency of the latest quantum bump beginning inside the response period. To make this estimate, we used the event latency distribution and the fact that the respective occurrences of quantum bumps in disjoint latency ranges are probabilistically independent. We further used the fact that, because of this independence, the probability of quantum bumps beginning between times x and y after a flash may be estimated as the number of flashes whose earliest event begins between x and y divided by the number of flashes without events beginning before x. The fraction of flashes f was thus estimated as $\int_t Pr$(quantum bumps begin between times t and $t + dt$) Pr(no quantum bumps begin beween $t + dt$ and the end of the response period) Pr(quantum bumps begin between the end of the response period and $t + dt + t_{sep}$), where the time parameter t ranged to the end of the response period and the integral was approximated as a sum over 20 ms intervals. For conservatively large values of t_{sep} (e.g., 160 ms for the cell of Fig. 2), the estimate for f turned out to be $< 3.1\%$ for Cell 2A and at least an order of magnitude lower for the other

TABLE I

Parameter Values for Experiments

Parameter	Cell 1	Cell 2A	Cell 2B	Cell 3	Cell 4
Holding potential (mV)	−52	−45	−45	−60	−60
Temperature (°C)	17.9	17.8	17.8	18.1	15.5
$[Ca^{2+}]_o$ (mM)	10	10	10	10	1
No. of flashes with stable data	3196	789	500	923	1084
Interflash interval (ms)	1350	2130	2130	1350	2520
Response period (ms)	80–340	60–340	60–340	80–280	140–920
Spontaneous (Spont.) q.b. observation period (ms)	0–50, 500–1350	700–2000	700–2000	500–1350	1000–2200
C_{min}, charge of the smallest reliably detected q.b. (pC)	4.0	4.0	4.0	4.0	6.0
$n_{R<}$, no. of responses with charge < C_{min}	39	4	2	3	7
$n_{R\geq}$, no. of responses with charge ≥ C_{min}	807	576	166	279	380
$n_{S<}$, no. of spont. q.b. with charge < C_{min}	30	7	19	17	0
$n_{S\geq}$, no. of spont q.b. with charge ≥ C_{min}	76	56	61	83	32
spont. q.b. arrival rate (s^{-1})	0.037	0.061	0.12	0.13	0.025
p_{OBS}, *Pr*(q.b. in response period)	0.265 ± 0.008	0.735 ± 0.016	0.336 ± 0.021	0.306 ± 0.015	0.357 ± 0.015
p_S, *Pr*(spont. q.b. in response period)	0.010	0.017	0.034	0.026	0.019
p_L, *Pr*(light-induced q.b. in response period)	0.258	0.730	0.312	0.287	0.344
w_L, *Pr*(response is purely light-induced)	0.964	0.977	0.897	0.915	0.946
w_S, *Pr*(response is purely spontaneous)	0.027	0.006	0.071	0.061	0.035
w_{LS}, *Pr*(response is both light-induced and spontaneous)	0.009	0.017	0.032	0.024	0.019
λ_{li}, mean no. of light-induced q.b. in response period	0.30	1.31	0.37	0.34	0.42
λ_S, mean no. of spont. q.b. in response period	0.010	0.017	0.034	0.026	0.019
$\lambda_{li,c}$, mean no. of light-induced q.b. given ≥ 1	1.16	1.79	1.20	1.18	1.23
p_{mult}, *Pr*(≥ 2 light-induced q.b. given ≥ 1)	0.142	0.516	0.176	0.160	0.196
Response charge range (pC)	0.4–568.9	0.7–1292.5	2.1–763.3	1.5–422.4	1.1–2203.1
m_{OBS}, mean response charge (pC)	79 ± 3	237 ± 8	205 ± 12	82 ± 4	159 ± 9
Spontaneous q.b. charge range (pC)	0.4–427.4	0.8–681.6	1.1–603.1	0.7–291.9	6.6–521.2
m_S, mean spontaneous q.b. charge (pC)	19 ± 5	106 ± 18	68 ± 13	29 ± 5	152 ± 26
m_L, mean light-induced q.b. charge (pC)	70 ± 3	132 ± 8	178 ± 12	72 ± 4	128 ± 9

For complete definitions, estimation and computation details, and additional notes, see Appendix E.

*q.b., quantum bump(s).

experiments. The estimated number of contaminated observed responses was f divided by p_{OBS} from Table I, or less than 4.2% for Cell 2A and at least five times lower for the other experiments. Moreover, typical quantum bumps were usually measured separately by our method even if their latencies differed by far less than t_{sep}. For this reason, the true numbers of contaminated observed responses were almost certainly much lower than the numbers just given. Even smaller were the numbers of observed responses contaminated similarly by quantum bumps beginning before the response period. Therefore, the net effect of inadvertently captured quantum bumps on the form of response charge distributions was negligible.

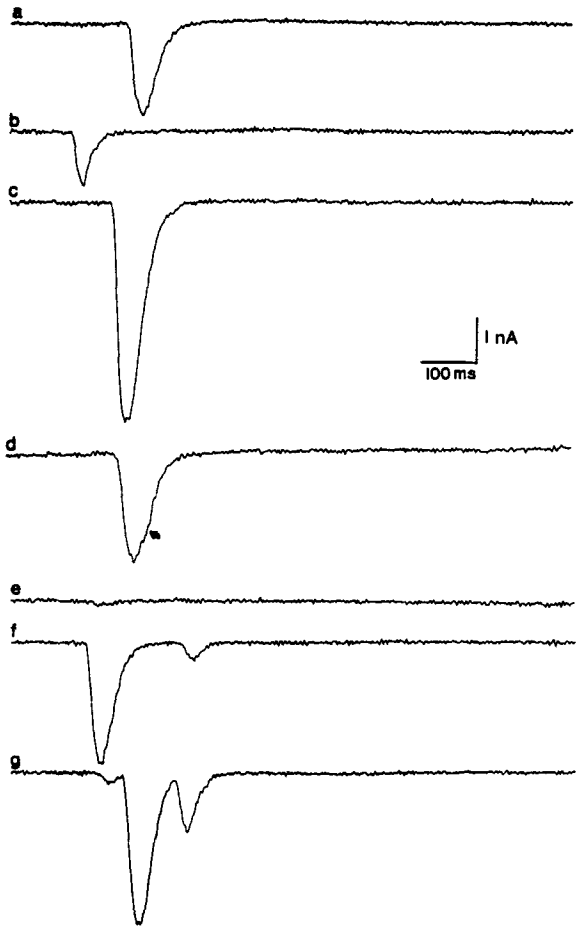

FIGURE 2. Voltage clamp current records showing quantum bumps evoked from Cell 1. A 3-ms flash was presented at the beginning of each trace. (*a–c*) Apparently individual quantum bumps. (*d*) Possibly two, superposed quantum bumps (note waveform near arrow). (*e*) One of the smallest quantum bumps detected by eye. (*f*) Apparently two quantum bumps. (*g*) Multiple, superposed quantum bumps.

To evaluate the resolution of our response charge measurements, we first considered the charges of the events with the smallest peak amplitudes ($\approx$0.1 nA) that could be reliably detected by eye above the recording noise. We thus identified a small, criterion charge, C_{min}, such that any event with charge greater than C_{min} was almost certainly detected (see Table I). In fact, as the table shows, some events smaller than C_{min} were detected, but, by far, most of the detected events were larger than C_{min}. Furthermore, C_{min} was much smaller than the average event charge. Thus, the measured responses with charge above C_{min} represented almost the entire charge range of interest. Moreover, the response charge distribution analysis was

specifically designed to take into consideration the very small events below C_{min} that were lost to measurement (see below). C_{min} proved to be much larger than the typical error in charge measurement, which was ascertained from the measurement of many traces that did not exhibit quantum bumps. Thus, smearing of response charge distributions by recording noise was negligible.

Statistical Methods

Tests for stability. The accurate measurement of statistically defined response parameters required temporal stability of the cell. Although we had screened for stability by eye during the experiment, we needed to expose and eliminate any nonobvious but statistically significant instabilities that remained in the data. The two most important stability indicators were the probability of response to a flash and the probability distribution of response charge. Two additional indicators were the rate of occurrence and charge distribution of spontaneous quantum bumps. Therefore, all these indicators were objectively examined for stability through specific statistical tests. A series of flashes that had been presented during a period of apparent stability was divided into sequential subseries. To test for long-term stability, three subseries of nearly equal numbers of flashes were used. To test for shorter-term stability, many more subseries, of ~100 flashes each (except possibly the last subseries), were used. In either case, a given stability indicator was evaluated for each subseries, and a statistic which measured the variability of the indicator across the subseries was computed (see below). To judge objectively whether the variability was too high for the cell to be considered stable, we evaluated the probability that the statistic would be at least as high as the value obtained if the cell were truly stable (significance probability). If the significance probability turned out to be very low (<0.01), then the hypothesis of stability was rejected. (If the significance probability was between 0.01 and 0.1, the deviation from stability was not necessarily significant in view of the number of such tests being done).

First we describe the stability test for the probability of response. Let m be the number of subseries, let k_j be the number of flashes in the j'th subseries for $j = 1, 2, \ldots, m$, and let r_j be the number of responses with charge at least C_{min} in the j'th subseries. Also, let $N_{1j} = r_j$, let $N_{2j} = k_j - r_j$ for $j = 1, \ldots, m$, let $n = \Sigma_{j=1}^{m} k_j$ be the total number of flashes, let $R_1 = J = \Sigma_{j=1}^{m} r_j$, and let $R_2 = n - J$. Then, the chi-square statistic

$$X^2 = n \sum_{i=1}^{2} \sum_{j=1}^{m} (N_{ij} - R_i k_j / n)^2 / (R_i k_j)$$

is a measure of the variability in the probability of response. X^2 has a discrete probability distribution, which we approximated by the distribution of a chi-square variable with $m - 1$ degrees of freedom (χ^2_{m-1}), as described by Bickel and Doksum (1977, p. 324). The hypothesis of stability was judged per above using the significance probability $Pr(\chi^2_{m-1} \geq X^2)$, where $Pr(H)$ denotes the probability of event H. Chi-squared significance probabilities were found using the algorithm of Holt (1986) and from published tables (Bevington, 1969).

We now describe the stability test for the distribution of response charge. The J responses with charge above C_{min} were ranked from 1 to J (tied charge values received their average ranks), and the Kruskal-Wallis test, suitably adjusted for ties (Bickel and Doksum, 1977, pp. 364, 397), was performed. This was a test of the hypothesis that each of the samples of r_j response charge values was taken from the same, unknown probability distribution (no assumptions were made on the form of the unknown distribution). Thus, Let $\bar{R}_j$ denote the average rank for the r_j responses in the j'th subseries, e the number of distinct charge values observed, and t_u the number of observations tied with the u'th distinct one, where $t_u \geq 1$ and

$t_u \equiv 1$ if all the observations are different. The Kruskal-Wallis statistic was defined as

$$T^* = \frac{\left[\frac{12}{J(J+1)}\sum_{j=1}^{m} r_j \bar{R}_j^2\right] - 3(J+1)}{1 - \frac{1}{J^3 - J}\sum_{u=1}^{e} t_u^3 - t_u}.$$

Its probability distribution was also approximated by that of χ^2_{m-1}. The approximation is acceptable if $r_j \geq 6$ for all j, or if $m > 3$ and $r_j \geq 5$ for all j, according to Bickel and Doksum (1977, p. 364). Adjoining subseries were combined, starting with the earliest ones, as necessary to obtain these conditions. The hypothesis of stability was rejected if T^* was too large, in the same sense as described above.

If the response charge distribution turned out to be significantly unstable by the Kruskal-Wallis test, then pairs of subseries i and j were compared by the two-sample Kolmogorov-Smirnov test (Darling, 1957). This is a test of the hypothesis that two samples come from the same, unknown probability distribution. The Kolmogorov-Smirnov test required calculation of the statistic

$$K^* = \max\left[\text{abs}\left(\frac{c_i(x)}{r_i} - \frac{c_j(x)}{r_j}\right)\right],$$

where $c_i(x)$ and $c_j(x)$ are the respective counts in subseries i and j of the responses with charge between C_{min} and x. This statistic was thus the maximum difference between the empirical cumulative conditional response charge probability distributions, given $x \geq C_{min}$, for subseries i and j, respectively. Significance probabilities of the Kolmogorov-Smirnov statistic K^* were obtained from Kim and Jennrich (1973). The respective Kolmogorov-Smirnov statistics for pairs of subseries and the respective mean response charge values for the individual subseries indicated which of the subseries deviated most from the others. When such a subseries was the first or last, it was deleted and the remaining subseries reexamined for stability as just described. When such a subseries was in the middle of the whole series, the data to one side of this subseries were discarded and the remaining data then reexamined.

Similar stability tests were also performed for the rate and charge distribution of spontaneous quantum bumps. Taken together, the stability tests revealed several instances of instability that had not been noticed by eye and thus prompted the discard of some (sometimes up to one third) of the recorded data. We report only results for data which had passed both the long- and shorter-term stability tests for all four indicators, with the one exception noted for Cell 4 in Appendix E (Details for Table I).

Estimating cascade model parameters and fitting models to response charge distributions. We tested predicted charge distributions using chi-squared tests (Bevington, 1969, p. 187), which involved the estimation of model parameters through the minimization of a chi-square statistic. Thus, for each experiment, we formed a total of m intervals, or "categories," of response charge x, with boundaries 0 pC $= x_0 < x_1 = C_{min} < x_2 < \cdots < x_m$. Nonresponses were included in the count for the lowest category, $0 \leq x < C_{min}$. To determine the category boundaries above C_{min}, we first formed equal bins of 10 pC $\leq x <$ 20 pC, 20 pC $\leq x <$ 30 pC, and so on, as well as a lowest bin $C_{min} \leq x <$ 10 pC. Then, beginning with the lowest bin, consecutive bins were combined to give eight categories, each with a roughly equal number of observations and thus comparable statistical weight. Thus, there were $m = 9$ categories in all for each experiment. Because of the low flash intensities used, there were many nonresponses and thus the lowest category, $0 \leq x < C_{min}$, contained many more observations than any of the others.

To define the chi-square statistic, let n_i be the number of observed response charge values in

the i'th category, $x_{i-1} \leq x < x_i$, and, for a given cascade model, let a_i be the theoretical probability that an observed response charge is in the i'th category. Then, the chi-square statistic, which is a measure of the deviation of the observations from the theory, is

$$X^2 = \sum_{i=1}^{m} (n_i - a_i n)^2/(a_i n),$$

where we note that $\Sigma_{i=1}^{m} n_i$ equals the total number of flashes n. For each model, a_i will be a function, $a_i = a_i(\theta)$, where θ is an unknown vector of parameters, say of dimension d. Let X^2_{min} denote the minimum value of X^2 over all possible values of θ. The vector θ is estimated by $\hat{\theta}$, the value of θ at which X^2_{min} is attained. If the theory being tested is correct (for some, unknown value of θ) and the model has d independent parameters, then the distribution of X^2_{min} can be approximated by that of a chi-square variable with $m - 1 - d$ degrees of freedom, χ^2_{m-1-d} (Bickel and Doksum, 1977, p. 320). Thus, the theory would be rejected if X^2_{min} is too large, i.e., if the significance probability $Pr(\chi^2_{m-1-d} \geq X^2_{min}) \leq 0.05$.

For our tests of theoretical response charge distributions, the probabilities a_i were equal to $V_R^{cum}(x_i) - V_R^{cum}(x_{i-1})$, where $V_R^{cum}(x)$ is the cumulative response charge distribution defined in Appendix A in terms of light-induced and spontaneous quantum bump quantities. The spontaneous quantum bumps beginning in the response period were both rare and much less frequent than light-induced quantum bumps (see Table I). This enabled us to calculate the a_i through the simplifying approximation of Eq. A4, which in essence treats the spontaneous quantum bumps as a small effect on top of the light-induced data. For the theoretical response charge distribution derived from the Scheme A cascade model (Results), the expression for $V_{\lambda_{li}}^{cum}$ in Eq. A4 is given by $V_{\lambda_{li},A}^{cum}$ in Eq. B12 of Appendix B; for the Scheme B model, $V_{\lambda_{li}}^{cum}$ is given by $V_{\lambda_{li},B}^{cum}$ in Eqs. C14–15 of Appendix C. The expressions in these equations were calculated by computer. We estimated the terms $V_{sqb}(x)$ and p_S in Eq. A4 (probability density for spontaneous quantum bump charge and the probability of occurrence of spontaneous quantum bumps in the response period) based on measurements of the events of the spontaneous quantum bump observation period (we did not assume any theory for the generation of spontaneous quantum bumps). Thus, we directly measured the empirical cumulative distribution of spontaneous quantum bump charge, denoted $V_S^{cum}(x)$, and calculated from $V_S^{cum}(x)$ an approximate, discrete estimate for $V_{sqb}(x)$ consisting of a set of probabilities at representative charge values. p_S was estimated as in Table I. The convolution in Eq. (A4) was actually performed only for Cell 2A; for the other experiments, it was sufficient to approximate the convolution based on our estimate that of the few observed responses containing a spontaneous quantum bump, only one third or fewer also contained light-induced quantum bumps (see w_L, w_{LS}, and w_S in Table I). Thus, we approximated that when a spontaneous quantum bump of charge $\geq C_{min}$ occurred in the response period, it occurred alone, and that any spontaneous quantum bump of charge $< C_{min}$ contributed negligibly (i.e., zero) to measured response charge. With the exception of Cell 2A, then, the convolution term in A4 was reduced to the set of probabilities

$$(p_S - p_{S\geq})[V_{\lambda_{li}}^{cum}(x_i) - V_{\lambda_{li}}^{cum}(x_{i-1})] + (p_{S\geq})[V_{sqb}^{cum}(x_i) - V_{sqb}^{cum}(x_{i-1})],$$

where $p_{S\geq}$ is the probability that a spontaneous quantum bump with charge $\geq C_{min}$ begins in the response period.

RESULTS

An important goal of our experiments was to measure the charge distribution of light-induced quantum bumps in *Limulus* ventral photoreceptors. The size variability

of these quantum bumps is evident from Fig. 2. Because multiple quantum bumps evoked by the same flash can temporally overlap and be mistaken for a single quantum bump (Fuortes and Yeandle, 1964; Lederhofer, Schnakenberg, and Stieve, 1991), it is not possible to determine the charge distribution rigorously by direct measurement of individual quantum bumps. We therefore sought an alternative method that would be based on parameters that could be measured with greater certainty. One parameter that can be measured with great accuracy is the total charge (response charge) generated by all the quantum bumps (light-induced and spontaneous) that begin during the response period, a period during which virtually all light-induced quantum bumps occur (Fig. 1). Response charge is of interest because its distribution can be calculated from the distribution for the charge of a single light-induced quantum bump (Appendix A). The basis for this calculation is that light-induced and spontaneous quantum bumps contribute independently to measured responses (Srebro and Yeandle, 1970), that a small number of quantum bumps add linearly under voltage clamp (Lisman and Brown, 1975), and that the total number of light-induced quantum bumps per flash obeys the Poisson distribution (Lillywhite, 1977). The calculation requires knowledge of the rate and charge distribution of spontaneous quantum bumps and the probability of a light-induced response, all of which can be accurately measured. It is therefore possible to examine a model for the charge distribution of a light-induced quantum bump by calculating the theoretical distribution of response charge on the basis of the model and comparing the calculated distribution to the observed one. Using this approach, the model can be accepted or rejected on sound, objective grounds.

In four cells, we were able to obtain data that met the stability criteria defined in Materials and Methods. Cell 2 yielded two sets of data, at two different intensities, respectively (Cell 2A and Cell 2B), giving a total of five experiments (see Table I). The response charge distributions for the five experiments are presented in Table II and plotted as average probability density in Fig. 3 (*bars*). The count in the lowest charge category (category 1) is the sum of two numbers: the number of flashes for which no response was detected (nonresponses) and the number of responses with charge below a small criterion value for reliable event detection, C_{min} (4–6 pC; see Materials and Methods and Table I). For all experiments except Cell 2A, the empirical probability of response (p_L) was low (≤ 0.34). Furthermore, the empirical probability of spontaneous quantum bumps beginning in the response period (p_S) was very low (≤ 0.034). Therefore, for Cells 1, 2B, 3, and 4, most ($\geq 80\%$) of the observed responses consisted of a single light-induced quantum bump and the response charge distribution above C_{min} was not very different from the light-induced quantum bump charge distribution. It can be seen from Fig. 3 that light-induced quantum bump charge is highly variable and not obviously quantized. On a more detailed level, the figure suggests that the probability density for light-induced quantum bump charge monotonically decreases with charge for Cell 1 but may have a more peaked form for the other experiments.

An important goal was to determine whether the measured distributions agreed quantitatively with the predictions of simple transduction cascade models. Such models would be unlikely to describe fully all the complexities of transduction, but, as argued in the Discussion, could capture essential aspects of the first stage of

TABLE II

Experimental and Theoretical Response Charge Distributions

Response charge		Experiment	Scheme A		Scheme B	
Category	Range (pC)	No. observed	No. expected	χ^2 contribution	No. expected	χ^2 contribution
Cell 1						
1	0–4	2389	2386.51	0.003	2386.51	0.003
2	4–10	91	65.41	10.008	65.41	10.008
3	10–20	86	93.09	0.540	93.09	0.540
4	20–30	80	78.47	0.030	78.47	0.030
5	30–50	110	130.08	3.099	130.08	3.099
6	50–70	94	100.55	0.427	100.55	0.427
7	70–100	109	109.50	0.002	109.50	0.002
8	100–150	110	110.79	0.006	110.79	0.006
9	150–∞	127	121.59	0.240	121.59	0.240
Cell 2A						
1	0–4	213	204.26	0.374	211.26	0.014
2	4–70	102	129.42	5.808	103.46	0.021
3	70–140	109	111.86	0.073	116.05	0.428
4	140–210	99	88.04	1.366	96.68	0.056
5	210–280	71	68.03	0.130	75.12	0.226
6	280–350	61	51.20	1.878	55.83	0.479
7	350–420	46	38.14	1.618	40.53	0.737
8	420–490	36	28.01	2.278	28.77	1.815
9	490–∞	52	70.05	4.652	61.29	1.408
Cell 2B						
1	0–4	334	324.85	0.258	332.03	0.012
2	4–40	20	29.77	3.209	17.10	0.493
3	40–100	21	36.63	6.672	33.56	4.703
4	100–130	19	14.50	1.393	16.28	0.454
5	130–170	21	15.81	1.700	19.00	0.210
6	170–210	20	13.86	2.717	16.96	0.543
7	210–280	21	18.16	0.445	22.11	0.055
8	280–370	23	16.01	3.055	18.26	1.230
9	370–∞	21	30.40	2.905	24.70	0.554
Cell 3						
1	0–4	644	637.70	0.062	643.62	0.000
2	4–20	42	54.97	3.060	39.99	0.101
3	20–40	43	50.84	1.210	47.76	0.475
4	40–60	42	38.90	0.247	42.45	0.005
5	60–80	36	30.40	1.032	35.33	0.013
6	80–100	31	23.74	2.217	28.04	0.312
7	100–120	25	18.59	2.214	21.68	0.508
8	120–170	30	30.92	0.028	34.00	0.471
9	170–∞	30	36.94	1.303	30.118	0.000
Cell 4						
1	0–6	704	696.50	0.081	703.18	0.001
2	6–30	36	58.74	8.803	35.34	0.012
3	30–60	53	59.26	0.661	54.71	0.053
4	60–90	53	48.86	0.350	54.10	0.023
5	90–120	46	40.30	0.807	47.50	0.047
6	120–150	49	33.67	6.977	40.06	1.993
7	150–190	42	34.64	1.563	40.73	0.040
8	190–290	51	55.31	0.336	60.73	1.558
9	290–∞	50	56.71	0.795	47.65	0.116

Number observed, number expected (for best fit), and χ^2 contribution are n_i, na_i, and $(n_i - na_i)^2/(na_i)$, as defined in Materials and Methods. The best fits are summarized in Tables III and IV and plotted in Fig. 3. For Cell 1, Scheme B fit best when one of the two active metarhodopsin states was altogether ineffective, i.e., when Scheme B reduced to Scheme A (see Table III and corresponding section of Appendix E). Thus, the best fits for the two models are identical for Cell 1.

amplification, which is probably the most important determinant of quantum bump size variability.

Scheme A

We first studied the simplest transduction cascade model (Scheme A; see Fig. 4), which is a generalization of the first stochastic cascade model for invertebrate

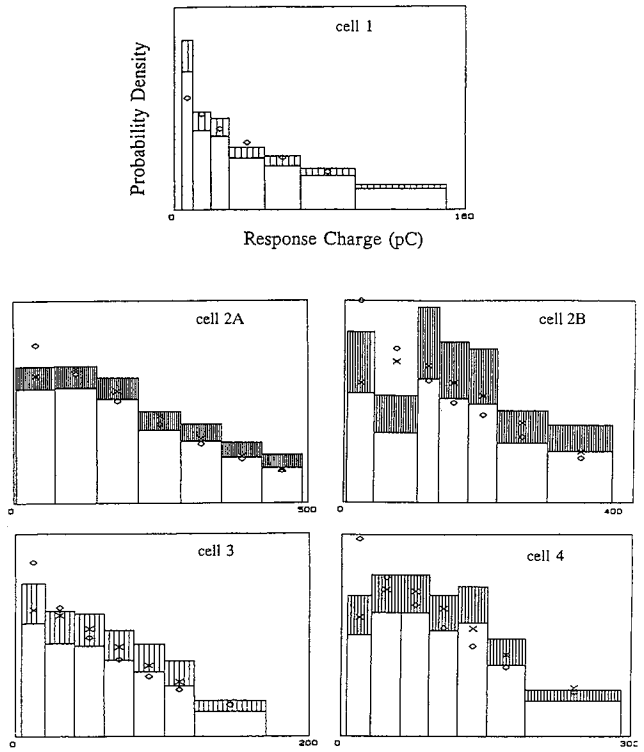

FIGURE 3. Experimental and theoretical response charge distributions. The number observed and number expected from each of categories 2 through 9 of Table II are plotted as average probability density, i.e., after dividing by the number of flashes (n from Table I) and the width of the category's charge range. The number observed corresponds to the middle of the striped region of a bar, where the striped region indicates ± one standard deviation = $\pm \sqrt{n_i(n_i/n)[1 - (n_i/n)]}/[n(x_i - x_{i-1})]$ (see Materials and Methods for notation). The number expected refers to the best fit of Scheme A (*diamond*) or Scheme B (*cross*). Notes: the number observed and number expected from category 1 would be off scale and hence are not plotted; the plotted value for category 9 is always 0 because the category extends to infinite charge; the best fits of Schemes A and B coincide for Cell 1 (see Table II, caption).

transduction (Borsellino and Fuortes, 1968). In Scheme A, amplification is produced in a sequence of stages. Thus, photoisomerization leads to an active molecule, E_1^*, which we take to be metarhodospin in its active state (M^*). In the first stage, M^* catalyzes the conversion of inactive molecules E_2 to an active form E_2^* (e.g., activated G protein). Each activation $E_2 \rightarrow E_2^*$ constitutes a unit of gain production by M^*. In

the second stage, each E_2^* catalyzes the conversion of inactive molecules E_3 to an active form E_3^*, and so on. In the next-to-last stage, molecules of second messenger E_{n-2}^* activate (open) light-sensitive channels ($E_{n-1} \rightarrow E_{n-1}^*$; Bacigalupo et al., 1986). In the last stage, each open channel E_{n-1}^* conducts extracellular ions into the cell ($E_n \rightarrow E_n^*$). All active molecules eventually become inactivated. Thus, metarhodopsin and all other active molecules are shut off, second messenger is removed, and channels close ($M^* \rightarrow M^o$ and $E_i^* \rightarrow E_i^o$, $i = 2, 3, \ldots n - 1$). The output of the cascade is defined as the total ionic charge that enters the cell, and therefore equals the total number of E_n^*s times the ionic charge per E_n^*.

In Scheme A, every gain-producing molecule E_i^* is shut off in a single step. This means that the molecule works in a single active state that produces gain stochastically as follows. Once active, the E_i^* can either produce a unit of gain (activate an E_{i+1}) or become inactivated. Whether gain production occurs before inactivation is a matter of chance. Thus, there is some probability p_i that the E_i^* will produce a unit of gain. If this happens, the E_i^* will next either produce a second unit of gain or become

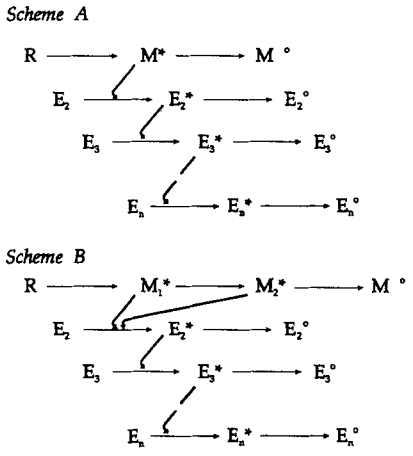

FIGURE 4. Simple transduction cascade models (Schemes A and B). (R) Rhodopsin molecule. (M^*) Single active metarhodopsin state. (M_1^* and M_2^*) Two, sequential active metarhodopsin states. (M^o) The inactivated form of metarhodopsin. (E_2, E_2^*, and E_2^o) The inactive precursor, active state, and inactivated forms, respectively, of the gain-producing molecules of stage 2. Similarly for stages 3 through n.

inactivated. Again, there is a probability p_i of gain production before inactivation, and so on. The invariance of p_i with the amount of gain already produced is an important, simplifying assumption. It is called here the "linear gain assumption" because it implies that active molecules, their substrates and products have no cooperative, saturation or other non-linear interactions that would affect the quantity of gain. The linear gain assumption does not exclude nonlinear interactions that would affect the *kinetics* of gain production as long as the probability p_i is not time-dependent.

To calculate the probability distribution for the total charge output of Scheme A, we first calculate the distribution for the gain produced by the active metarhodopsin molecule, M^*, of stage 1. For M^* to activate a total of n E_2s means that M^* activates n E_2s in succession and is then inactivated. By the linear gain assumption, these successive activation and inactivation events are probabilistically independent. Therefore, with p_1 being the probability that M^* (E_1^*) will next activate an E_2 rather than become inactivated, the probability for a total of n E_2 activations equals $(p_1)^n(1 - p_1)$, a geometric probability (Ross, 1972, p. 24). We may likewise reason that a single E_2^*

will produce a geometrically distributed number of E_3^*s. To deduce the distribution for the total number of E_3^*s, however, is relatively complicated, because we must somehow take into account the fact that the population of E_3^*s is produced by a random number of E_2^*s. How much more complicated, then, will it be to deduce the distribution for the output of the entire cascade? Remarkably, there is an elegant way to fold together the randomness in gain production from all the stages (see Appendix B), with a simple result: the charge distribution for the output of Scheme A consists of a probability at zero charge and an exponential distribution above zero charge (Eq. B10). The probability at zero charge signifies that the cascade can fail to generate a quantum bump (cascade failure). The probability of cascade failure stems from the possibility that, as mentioned above, an active molecule can fail to produce any gain before becoming inactivated (molecular failure). Thus, M^* could become inactivated before producing any E_2^*s (probability $1 - p_1$), in which case the cascade would abort at stage 1. Alternatively, M^* could produce E_2^*s which all fail to yield E_3^*s, or all molecules activated in some later stage could fail. The probability of cascade failure is an important result because it signifies that the quantum efficiency of transduction will be less than the quantum efficiency of isomerization (probability that absorption leads to M^*; Fein and Szuts, 1982). Thus, a noteworthy parameter of the Scheme A model is the quantum efficiency given that rhodopsin has been photoactivated to M^*. This parameter is denoted here QE_A and equals one minus the probability of cascade failure.

The exponential distribution above zero charge (see Eq. B10) is the charge distribution for a light-induced quantum bump of Scheme A. Appendix B proves the exponential for all possible Scheme A mechanisms (a complementary proof for many of these mechanisms is given by Grzywacz and Hillman, 1985). In particular, Appendix B shows why an exponential, and not some other distribution form, is obtained regardless of the number of cascade stages and reaction time constants. The exponential has a single parameter, which is the mean light-induced quantum bump charge ($m_{L,A}$).

Based on the exponential distribution for light-induced quantum bump charge, we calculated the distribution of response charge for Scheme A as described in Materials and Methods. The response charge distribution has two free parameters, the mean light-induced quantum bump charge, $m_{L,A}$, and the mean number of light-induced quantum bumps beginning in the response period, $\lambda_{li,A}$. Both parameters together influence the form of the response charge distribution above zero charge, but $\lambda_{li,A}$ alone influences the predicted count at zero charge (number of nonresponses), which is included in the lowest distribution category (category 1). For each experiment, we varied the two parameters jointly to obtain the best fit to the data of all the categories (Table II; Fig. 3, *diamonds*). The best fit corresponded to the minimum value of the chi-square statistic X^2 (see Materials and Methods), X^2_{min}. The values of $\lambda_{li,A}$ and $m_{L,A}$ that gave the best fit served as the experimental estimates for these parameters and are listed in Table III. For each experiment, the estimate for $\lambda_{li,A}$ is quite close to the estimate for the analogous, model-independent parameter λ_{li} (Table I), where the latter estimate is derived purely from the observed number of nonresponses and the Poisson distribution (see Appendix E). It should be noted, however, that varying

TABLE III

Values of Independent and Implied Parameters of Schemes A and B for the Best Fits to Response Charge Data

Quantity	Cell 1	Cell 2A	Cell 2B	Cell 3	Cell 4
Scheme A, independent parameters:					
$\lambda_{li,A}$, mean number of light-induced quantum bumps in response period	0.3026	1.28	0.414	0.369	0.44467
$m_{L,A}$, mean light-induced q.b. charge (pC)	67.14	126.9	174.2	69.2	119.3
Scheme A, implied parameters:					
SD/mean of light-induced q. b. charge	1.0	1.0	1.0	1.0	1.0
Scheme B, independent parameters:					
$m_{M_1^*}$ mean charge output from a successful M_1^* cascade (pC)	arbitrary	52.4	85.7	35.5	39.5
$m_{M_2^*}$ mean charge output from a successful M_2^* cascade (pC)	67.14	97.32	102.1	45.7	89.9
ξ	0.0	−0.977088	−1.743	−0.85206	−0.27663
η	0.3026	2.30	2.128	1.201	0.696
Scheme B, implied parameters:					
$f_{M_1^*}$, $Pr(M_1^*$ cascade fails)	—	0.214	0.071	0.080	0.084
$f_{M_2^*}$, $Pr(M_2^*$ cascade fails)	—	0.115	0.060	0.062	0.037
QE_B, q efficiency given photoactivation	—	0.975	0.996	0.995	0.997
$\lambda_{li,B}$, mean no. of light-induced q.b. in response period	0.3026	1.303	0.385	0.349	0.419
$m_{E_2^*}$ mean charge successful E_2^* cascade (pC)	—	11.2	6.1	2.84	3.32
$m_{L,B}$, mean light-induced q.b. charge (pC)	67.14	130.3	176.3	75.9	123.2
SD/mean of light-induced q.b. charge	1.0	0.834	0.753	0.759	0.787

For details, see Appendix E.
q.b., quantum bump.

$m_{L,A}$ and $\lambda_{li,A}$ jointly, as we did, yields a fit that is at least as good as, and probably better than, the fit that would follow from first setting $\lambda_{li,A}$ to λ_{li} and then varying $m_{L,A}$ alone to get a X^2_{min} for the data above C_{min} (a conceptually simpler, though approximate approach).

To judge the overall fit objectively, we evaluated the significance probability that corresponds to X^2_{min} (Table IV). This is the probability that if the model is correct, X^2_{min} will be at least as large as the value actually obtained. Thus, a very small

TABLE IV

Chi-Square Minima and Significance Probabilities for Fits of Cascade Models to Response Charge Data

Cell	Scheme A		Scheme B	
	X^2_{min}	Significance probability	X^2_{min}	Significance probability
1	14.35	0.026	14.35	0.00626–0.026
2A	18.18	0.00580	≤5.18	≥0.269
2B	22.35	0.00105	≤8.26	≥0.0826
3	11.37	0.0775	1.88	0.757
4	20.37	0.00238	3.84	0.428

See Appendix E for details.

significance probability for some experiment would prompt rejection of the model for that experiment. Table IV indicates that the experiment most supportive of Scheme A is Cell 3, but even for that experiment, the fit to the response charge distribution was only marginal (Fig. 3). A worse, and unacceptable fit was obtained for Cell 1, which is seen to have yielded many more small responses than expected on the basis of Scheme A (Fig. 3). Very bad fits were obtained for Cells 2A, 2B and 4, which, in contrast to Cell 1, yielded fewer responses at low charge values and more responses at intermediate charge values than expected (a relatively peaked distribution; Fig. 3). Therefore, the pooled results from all the experiments lead to the strong conclusion that Scheme A should be rejected as a transduction model. This conclusion differs from that of Grzywacz and Hillman (1985), who found that an exponential yields good fits to light-induced quantum bump charge distributions from *Limulus*. Possible reasons for the difference between their and our conclusions are presented in the Discussion.

Scheme B

Having found that Scheme A failed to account for the observed response charge distributions, we sought a simple modification of Scheme A that would lead to consistency with the data. One of the simplest modifications is to replace the single step of metarhodopsin inactivation with a two-step inactivation process (e.g., phosphorylation followed by arrestin binding; Wilden, Hall, and Kuhn, 1986). Therefore, we considered a second cascade model (Scheme B; see Fig. 4) in which metarhodopsin passes sequentially through two, independent active states, M_1^* and M_2^*. Scheme B is identical to Scheme A after the photopigment stage.

Scheme B can be viewed as the sum of two, separate cascades, one initiated by M_1^* and the other, by M_2^*. The M_1^* cascade comprises M_1^*, all the E_2^*s it activates, all the E_3^*s they activate, and so on, through any resulting output. Similarly, the M_2^* cascade comprises M_2^*, all the E_2^*s it activates, all the E_3^*s they activate, and so on. Like the active molecules of Scheme A, M_1^*, M_2^* and all the active molecules of Scheme B's subsequent stages are assumed to produce gain according to the linear gain assumption articulated in the description of Scheme A. Therefore, the M_1^* and M_2^* cascades proceed independently and yield probabilistically independent outputs. In fact, each of these cascades has gain production properties identical to those of Scheme A. Therefore, each cascade has some probability ($f_{M_1^*}$ and $f_{M_2^*}$, respectively) of failing to produce any output; likewise, each cascade has a certain probability ($1 - f_{M_1^*}$ and $1 - f_{M_2^*}$) of yielding an exponentially distributed output (respective means $m_{M_1^*}$ and $m_{M_2^*}$). The output of Scheme B is the sum of the M_1^* and M_2^* cascade outputs, and therefore varies probabilistically among four types: (*a*) zero (Scheme B failure; probability $f_{M_1^*} \times f_{M_2^*}$); (*b*) exponentially distributed with mean $m_{M_1^*}$ (probability $[1 - f_{M_1^*}] \times f_{M_2^*}$); (*c*) exponentially distributed with mean $m_{M_2^*}$ (probability $f_{M_1^*} \times [1 - f_{M_2^*}]$), and; (*e*) distributed as the sum of two exponential contributions (a peaked distribution with mean $m_{M_1^*} + m_{M_2^*}$; probability $[1 - f_{M_1^*}] \times [1 - f_{M_2^*}]$). The quantum bump charge distribution for Scheme B is the weighted superposition of the distributions for the last three types. Details are given in Appendix C. Among the most important points explained there is that the quantum bump charge distribution can range from a monotonically decreasing form (output types 2 and/or 3 dominate)

to a form with a single peak (type 4 dominates). The monotonically decreasing form is obtained, for example, when both M_1^* and M_2^* produce relatively low gain, and even becomes exponential when one of these states produces very low gain (Scheme B effectively reduces to Scheme A). The peaked form of the distribution results when both M_1^* and M_2^* produce relatively high gain. It is the ability of Scheme B to yield not only the monotonically decreasing form, but also the peaked form that distinguishes the character of its prediction from that of Scheme A's.

As explained in Appendix C, the response charge distribution for Scheme B has four independent parameters (Table III). For each experiment, we varied these parameters jointly to minimize the value of the chi-square statistic X^2 (Table II; Fig. 3, *crosses*). The significance probabilities in Table IV indicate that Scheme B yields excellent fits for Cells 2A, 3 and 4, and a marginal, though acceptable, fit for Cell 2 *B*. For Cell 1, however, Scheme B does not fit the data any better than Scheme A, and, given Scheme B's greater number of free parameters, its fit is judged as especially poor (significance probability between 0.006 and 0.026). In fact, under the hypothesis of Scheme B, it is unlikely (probability between 0.03 and 0.13) for even one out of five independent experiments to yield such a bad fit (see Appendix E regarding Table IV). Thus, the pooled results from all five experiments suggest that Scheme B can account for the light-induced quantum bump charge distribution in most, but not all, cells.

The striking difference between Cell 1 and the other experiments led us to inquire whether Cell 1 was somehow atypical in its transduction properties. Previous workers have reported that latency and size are uncorrelated (Stieve and Bruns, 1983; Howard, 1983). To study if this was true in our data, we examined the charges of early and late events (Table V), choosing early and late latency ranges (e.g., for Cell 1, 80–110 and 240–270 ms), such that the respective numbers of events beginning in the two ranges were large enough for a meaningful statistical comparison and such that relatively few of the events were expected to contain spontaneous quantum bumps (e.g., for Cell 1, ≤ 3.5 events out of 44). Even if quantum bump latency and size were uncorrelated, one would expect early events to tend to have higher total charge than late events because an early quantum bump is more likely than a late quantum bump to be followed by a second, superposing quantum bump. The significance probabilities of Table V, however, indicate just the opposite type of correlation for Cell 1 (early events were smaller). By contrast, we found no evidence of correlation for Cells 2A, 3, and 4, and only a marginal possibility that early events were larger than late events in Cell 2B. Thus, we infer a correlation between latency and size for the light-induced quantum bumps of Cell 1 that contrasts with the correlation properties of our other cells and cells studied previously. Cell 1 may thus be atypical in its transduction properties (see Discussion).

DISCUSSION

The underlying question of this paper is why identical photons produce responses (quantum bumps) of highly variable size in *Limulus* ventral photoreceptors (Fig. 2). We have examined this problem by calculating quantum bump charge distributions predicted from simple cascade models. For the simplest models—those in which the gain-producing molecules of each stage are inactivated in a single step

(Scheme A, Fig. 4, and Appendix B)—we drew two fundamental conclusions. The first is that the cascade will sometimes fail to produce a quantum bump (quantum efficiency < quantum efficiency of isomerization). This will be true for any cascade in which gain is produced through the simple kinds of molecular active states we have considered. The second conclusion, consistent with the findings of Grzywacz and

TABLE V

The Relationship Between Event Latency and Charge

	Cell 1	Cell 2A	Cell 2B	Cell 3	Cell 4
Latency range for early events (ms)	80–110	60–100	60–140	80–120	140–260
Latency range width for early events (ms)	30	40	80	40	120
M, number of early events	47	16	33	39	45
Expected number of early events containing a spontaneous quantum bump	3.5	1.9	4.9	4.7	2.2
Mean ± standard deviation of early event charge	45.4 ± 72.7	278.4 ± 205.9	238.8 ± 198.4	67.9 ± 61.2	161.7 ± 195.3
Latency range for late events (ms)	240–270	300–350	230–310	200–240	520–640
Latency range width for late events (ms)	30	50	80	40	120
N, number of late events	44	16	33	39	41
Expected number of late events containing a spontaneous quantum bump	3.5	2.4	4.9	4.7	2.2
Mean ± standard deviation of late event charge	84.7 ± 72.5	175.5 ± 168.4	148.6± 105.8	68.9 ± 43.5	133.5 ± 118.3
$K^* =: \max\left[\text{abs}\left(\frac{c_e(x)}{M} - \frac{c_l(x)}{N}\right)\right]$	0.3810445	0.3125	0.3030303	0.2307692	0.1436314
Significance probability (Pr) for K^*	$0.001 < Pr < 0.005$	$Pr > 0.1$	$Pr = 0.1$	$Pr > 0.1$	$Pr > 0.1$
Linear-correlation coefficient for event latency and charge for all early and late events combined	0.277409	−0.267702	−0.2484745	−0.03517751	−0.05333124
Significance probability (Pr) for linear-correlation coefficient	$Pr < 0.01$	$Pr > 0.1$	$Pr = 0.05$	$Pr \gg 0.1$	$Pr \gg 0.1$

K^* is a Kolmogorov-Smirnov statistic (Materials and Methods), with $c_e(x)$ and $c_l(x)$, respectively, the counts of early and late events with charge $\leq x$. The linear-correlation coefficient (Bevington, 1969, pp. 119, 310–312) was calculated for all early and late events combined.

Hillman (1985), is that quantum bumps generated by the cascade will have a charge distribution that is exponential in form. An exponential is very wide (standard deviation/mean = 1; Ross, 1972, p. 49), and implies progressively smaller numbers of quantum bumps at increasing charge values. Intuition might suggest that because the number of G proteins is discrete, the size distribution should consist of a series of

narrow peaks. Such peaks are absent, however, because random gain production after the G protein stage broadens any would-be peaks so much that on the scale of average quantum bump charge, they become completely obliterated. We emphasize that this broadening is a predicted effect of the cascade itself and has nothing whatsoever to do with experimental recording noise or measurement error.

Even by eye, the response charge data of Fig. 3 suggest that the light-induced quantum bump charge distribution is much closer to an exponential than, say, to a distribution that is highly peaked about its mean (standard deviation/mean $\ll 1$). On the other hand, four out of five data sets (Cells 2A, 2B, 3, and 4) suggest some degree of peakedness, i.e., that the very smallest quantum bumps are not obviously the most numerous. Furthermore, even for low probabilities of response (Cells 1, 2B, 3, and 4) the response charge distribution will tend to be somewhat more peaked than the light-induced quantum bump charge distribution. Therefore, to decide whether the data are really consistent with an exponential and hence with the simplest cascade models requires rigorous statistical tests. We conducted chi-square tests for exponentiality and found that an exponential yields a marginal fit to one of our data sets (Cell 3), a bad fit to a second (Cell 1), and very bad fits to the remaining three (Cells 2A, 2B, and 4; see Fig. 3, *diamonds,* and Table IV). We have therefore concluded that it is not generally true that the charge distribution for light-induced quantum bumps is exponential. Consequently, the simplest cascade models for transduction are not adequate.

This conclusion differs from that of Grzywacz and Hillman (1985), who found consistency with an exponential in *Limulus.* Their experimental protocol differed substantially from ours, but we have no reason to attribute the difference in conclusions to the difference in protocol. One possibility we have examined is whether the different conclusions could have resulted from different numbers of charge distribution categories used to test theoretical predictions. Both our observed and model-based distributions suggest probability densities that change relatively slowly with charge. Accordingly, we used a small number of categories (nine), which both captured essential distribution characteristics and yielded a relatively large number of events per category, thus facilitating the exposure of significant differences with the theory. Indeed, the use of a larger number of categories can make an exponential appear to fit better (Lisman and Goldring, 1985), essentially because the chi-square test is not sensitive to whether categories with similar discrepancies between theory and data are adjacent (suggestive of a real model insufficiency) or widely separated (consistent with normal statistical fluctuation). Grzywacz and Hillman's (1985) Fig. 2 shows 36 bins, which presumably they grouped into 25 categories to meet the conditions for the chi-square test (Materials and Methods). When we regroup their data into nine categories (2.5–20, 20–40, 40–60, . . . pC), the fit of an exponential becomes marginal (significance probability ≈ 0.07), though not small enough in this one example to attribute the difference in conclusions to a difference in the number of categories. Moreover, even regrouping their data does not expose any obvious peaked distributional character of the type suggested by most of our data sets, or, as additional examples, data of Stieve, et al. (1990) and most of the data sets of the companion paper (Kirkwood, A. and J. E. Lisman, 1994). Thus, it seems that the light-induced quantum bump charge distribution can appear expo-

nential in some experiments and significantly more peaked in others. While the reasons for this are not clear, what is clear is that there is now a significant collection of charge distribution data for which the simplest cascade models alone cannot account.

Having rejected the simplest models, we next explored whether our data could be explained by a simple augmentation of Scheme A in which metarhodopsin passes through not one, but two, sequential active states (Scheme B: Fig. 4, and Appendix C). This scheme is suggested by other kinds of findings (see below), and is also among a general class of models with multiple active states that Grzywacz and Hillman (1985) discussed in connection with distribution peakedness (see below). Because Scheme B can reduce to Scheme A (the gain produced by one of the active metarhodopsin states can approach 0), Scheme B is automatically consistent with experimental distributions that are adequately described by an exponential, such as those of Grzywacz and Hillman (1985) and our Cell 3. Further, however, the distribution predicted by Scheme B can be more peaked than an exponential, as we have shown explicitly in Appendices C and D. This potential for a more peaked distribution did not enable Scheme B to fit Cell 1 any better than Scheme A (which did not fit well; see Fig. 3*A*), but did enable Scheme B to fit the other four experiments well (Fig. 3, crosses; Table IV), in contrast to Scheme A. On further examination of Cell 1, we found evidence (Table V) that quantum bump size and latency were correlated, unlike in the other cells and previously reported experiments (Stieve and Bruns, 1983; Howard, 1983). Cell 1's simultaneous anomalies in the quantum bump charge distribution and the correlation between quantum bump size and latency might be explained if Cell 1 were one of the relatively rare cells with two R-lobes (Stern, Chinn, Bacigalupo, and Lisman, 1982). Thus, one R-lobe might generate the small, early quantum bumps, and the other might generate the large, late quantum bumps. In the absence of independent evidence for this or any other explanation, however, we can say only that Cell 1 is anomalous in multiple respects and should therefore not be used to reject Scheme B. If we disregard Cell 1, Scheme B provides a satisfactory statistical explanation for the light-induced quantum bump charge distribution.

Scheme B is a very particular model that makes assumptions not only about the first cascade stage, but also about all subsequent stages. The assumptions about the subsequent stages, however, may not be of great consequence in accounting for the data. This is because output variability is due primarily to variability in the gain produced by the first stage provided the average gain of the first stage is reasonably high ($\gtrsim 10$), as is true in *Limulus* (Kirkwood, Weiner, and Lisman, 1989). An intuitive reason for this is that fluctuations in the respective contributions to cascade output from many G proteins will tend to cancel, leaving the main source of variability to be the random number of these contributions that add together (equal to the number of G proteins). Appendix D proves this concept mathematically for the variability indicator standard deviation/mean (see Grzywacz and Hillman, 1985, for related discussion), and then uses this indicator to show how the variability in the output of Scheme B can be understood directly in terms of the variability in the number of G proteins activated. Appendix D also explains why the variability in the number of G proteins may largely determine not just the standard deviation/mean, but nearly

the whole form of the quantum bump charge distribution. This is illustrated in Fig. 5, which compares the outputs of two cascades that have the same, highly stochastic first stage but quite different kinds of stochastic variability after the first stage. The quantum bump charge distributions for the two cascades are seen to be quite close over most of the charge range. These results suggest that even if late stages in the phototransduction cascade differ in important ways from the simple cascade modeled by Scheme B, the scheme may still capture the reactions that are the primary determinant of output size variability.

The two steps of metarhodopsin inactivation suggested by Scheme B are envisioned to be slow enough for metarhodopsin to have time to produce significant gain, but additional fast inactivation steps cannot be ruled out. On the other hand, it can

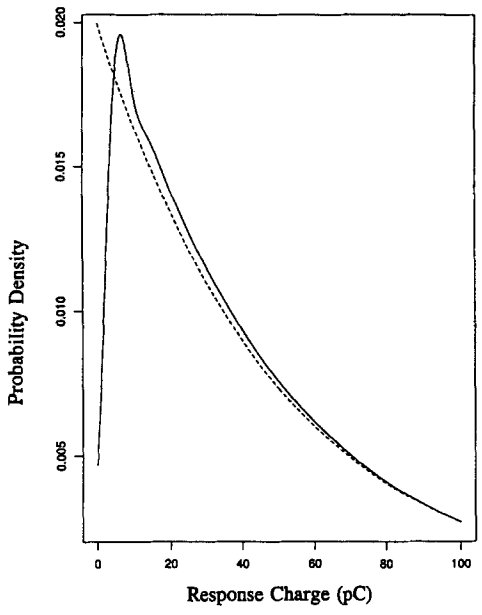

FIGURE 5. Illustration of the large influence of the first stage of amplification on the variability of light-induced quantum bump charge. Two models are considered. Both have an identical first stage in which a single active metarhodopsin state yields a geometrically distributed number of activated G proteins (G*), with an average of 10 G*s when a quantum bump is generated. In the model for the dotted curve, a G* stimulates a charge flow with a Gaussian distribution (peaked) that has mean 5 pC, variance 10 $(pC)^2$ and hence standard deviation/mean of 0.63. In the model for the dashed curve, a G* stimulates an exponentially distributed charge flow with mean 5 pC, variance 25 $(pC)^2$ and hence standard deviation/mean of 1. Both models yield the same mean quantum bump charge of 50 pC.

be argued (see below and Grzywacz and Hillman, 1985) that many high-gain-producing steps would lead to a highly peaked distribution, contrary to what we have found. Thus, our work suggests that metarhodopsin is turned off by a process that has more than one step of high gain production, but not many such steps.

The actual mechanism of metarhodopsin inactivation in *Limulus* is not known, but the following additional considerations also point towards a multistep inactivation process. First, the evidence from vertebrate systems, where the mechanism of metarhodopsin inactivation has been extensively investigated, suggests that both phosphorylation of metarhodopsin (Wilden and Kuhn, 1982; Sitaramayya and Liebman, 1983) and the binding of arrestin (Kuhn, Hall, and Wilden, 1984) must occur before the pigment is inactivated (Wilden et al., 1986). Both rhodopsin

phosphorylation (Vandenberg and Montal, 1984) and arrestin (Smith, Shieh, and Zucker, 1990; Yamada, Takeuchi, Komori, Kabayashi, Sakai, Hotta, and Matsumoto, 1990) are found in invertebrate photoreceptors, though their function is not yet established. Second, experiments in *Limulus* median eye (Lisman, 1985) have revealed a class of spontaneous quantum bumps whose size properties can be explained simply if metarhodopsin is inactivated in a sequence of steps. These spontaneous quantum bumps result from the reversal of metarhodopsin inactivation and are smaller than light-induced quantum bumps on the average. The size relationship between the two kinds of quantum bumps implies that the reversal of inactivation yields an active form of metarhodopsin that produces less gain than the form produced by the light-activated forward reaction. This suggests that the metarhodopsin resulting from the reversal of inactivation has only to undergo a final inactivation step to be shut off again, whereas a photoactivated metarhodopsin molecule must proceed through each of multiple inactivation steps, thereby having more time to activate G proteins. The reasoning outlined here is upheld even when stochastic variability is taken into account (Goldring, M. A., and J. E. Lisman, manuscript in preparation). A final reason for suspecting that metarhodopsin may be inactivated in multiple steps comes from a theoretical argument that shows that multi-step inactivation yields higher quantum efficiency than single-step inactivation (Goldring and Lisman, manuscript in preparation). Intuitively, the reason for the higher quantum efficiency is that fluctuations in the respective gain contributions from multiple active metarhodopsin states tend to cancel; thus, the distribution of first-stage gain is more peaked, and the probability of zero gain (which implies cascade failure) smaller, for multiple active states than for a single active state.

The companion paper (Kirkwood and Lisman, 1994) examines the charge distribution of quantum bumps under conditions where the fluctuations in output cannot be attributed to fluctuations in the number of G proteins activated. Under these conditions, the charge distribution appears much closer to exponential. This observation lends further support to the multi-step rhodopsin inactivation cascade model of this paper and, more generally, to the idea that the size variability of light-induced quantum bumps provides significant information about the first stage of amplification in transduction.

APPENDIX A

The Probability Distribution for Response Charge

Here we derive a general expression for the probability density of response charge, defined in the text, and an approximation for the cumulative response charge distribution that applies when spontaneous quantum bumps are both rare and much less frequent than light-induced quantum bumps.

The number of metarhodopsin molecules activated by a flash is Poisson distributed with some mean λ'. Each of these has some probability QE (the quantum efficiency given photoactivation) of stimulating a quantum bump, which has a large probability P_{RP} of beginning in the empirically defined response period (e.g., see Fig. 1). Because a small number of quantum bumps superpose linearly under voltage clamp (Lisman and Brown, 1975), the probability density for the summed charges of these quantum

bumps (the "light-induced response") is

$$V_{\lambda_{li}}(x) = \sum_{k=0}^{\infty} e^{-\lambda(QE)} \left(\frac{[\lambda(QE)]^k}{k!} \right) (V_{liqb})^{*k}(x), \tag{A1}$$

where $V_{liqb}(x)$ is the probability density for the charge of a light-induced quantum bump, $\lambda_{li} =: \lambda(QE) =: \lambda' P_{RP}(QE)$ is the mean number of light-induced quantum bumps beginning in the response period (see Ross, 1972, pp. 77–78, and cf Yeandle, 1958), $f^{*k}(x)$ denotes the k-fold convolution (Ross, 1972, p. 42) of a function f with itself, and a zerofold self-convolution is defined as the Dirac delta distribution δ_0:

$$\begin{aligned} \delta_0(x) &= 0, \quad x \neq 0, \\ \int_0^{+\epsilon} \delta_0(x)\, dx &= 1, \quad \epsilon > 0. \end{aligned} \tag{A2}$$

Similarly (see Srebro and Yeandle, 1970), the total charge of all the spontaneous quantum bumps beginning in the response period (the "spontaneous response") will have probability density

$$V_{\lambda_s}(x) = \sum_{k=0}^{\infty} e^{-\lambda_s} \left(\frac{(\lambda_s)^k}{k!} \right) (V_{sqb})^{*k}(x), \tag{A3}$$

where V_{sqb} is the probability density for the charge of a spontaneous quantum bump and λ_s is the mean number of spontaneous quantum bumps that begin in the response period. A measured response is the sum of the light-induced and spontaneous responses, and therefore response charge has probability density $V_R(x) = [V_{\lambda_{li}} * V_{\lambda_s}](x)$. The cumulative response charge distribution is $V_R^{cum}(x) = \int_{y=0}^{x} V_R(y)dy$. Note that for an infinitesimally small $\epsilon > 0$, $V_R^{cum}(\epsilon) = \int_0^{+\epsilon} e^{-\lambda_{li}} e^{-\lambda_s} \delta_0(x)dx = (1 - p_L)(1 - p_S)$, where $p_L =: 1 - e^{-\lambda_{li}}$ and $p_S =: 1 - e^{-\lambda_s}$ are, respectively, the probabilities that no light-induced quantum bumps and no spontaneous quantum bumps begin in the response period.

If $p_S \ll p_L$, then the number of spontaneous quantum bumps beginning in the response period is usually 0, rarely 1, and practically never >1, so $V_{\lambda_s}(x) \approx (1 - p_S)\delta_0(x) + (p_S)\, V_{sqb}(x)$, and we have the useful approximation

$$V_R^{cum}(x) \approx (1 - p_S)\, V_{\lambda_{li}}^{cum}(x) + (p_S) \int_{y=0}^{x} (V_{\lambda_{li}} * V_{sqb})(y)\, dy, \tag{A4}$$

where $V_{\lambda_{li}}^{cum}(x) =: \int_{y=0}^{x} V_{\lambda_{li}}(y)\, dy$ is the cumulative probability distribution for the charge of the light-induced response.

APPENDIX B

The Light-induced Quantum Bump Charge and Response Charge Probability Distributions for Scheme A

Scheme A is described in Results. Here we will first show that the probability distribution for the charge output of Scheme A consists of the probability $1 - QE_A$ at zero charge (cascade failure) and an exponential light-induced quantum bump charge distribution above zero charge (Eq. B10). Then we will give the corresponding cumulative charge distribution for a purely light-induced response (no spontaneous

quantum bumps; Eq. B12). Finally, we will remark briefly on the scope of the Scheme A activation and inactivation reaction mechanisms, which include those of the Borsellino-Fuortes (1968) model.

The light-induced quantum bump charge probability distribution for scheme A. Scheme A has $n - 1$ types of active molecules E_i^*, $i = 1, 2, 3, \ldots, n - 1$, with E_1^* the same as activated metarhodopsin, M*. An E_i^* produces only E_{i+1}^*s, and the number of E_{i+1}^*s produced by a given E_i^* has a distribution $\{p_{i,k}\}_{k=0}^{\infty}$ which does not depend on anything except i. Thus, the cascade is a multitype Galton-Watson branching process (Harris, 1963). Let f_i be the probability generating function (Feller, 1968, p. 264) for the distribution $\{p_{i,k}\}_{k=0}^{\infty}$:

$$f_i(s) = \sum_{i=0}^{\infty} p_{i,k} s^k, \quad |s| \leq 1. \tag{B1}$$

It can be shown (Harris, 1963, pp. 5, 36; Jagers, 1974) that because the cascade begins with a single molecule, E_1^*, the number of E_n^*s has a generating function

$$F_n(s) = f_1(f_2(\ldots(f_{n-1}(s)))\ldots). \tag{B2}$$

The definition of p_i given in Results implies that the $p_{i,k}$ are geometric probabilities

$$p_{i,k} = (p_i)^k(1 - p_i). \tag{B3}$$

For $k \geq 1$, the $p_{i,k}$ can be expressed in the form ab^{k-1}, with $a, b \geq 0$. We will call any such distribution "semigeometric." It can be shown (Harris, 1963, p. 9) that a probability distribution is semigeometric if and only if its generating function $G(s)$ is fractional-linear, i.e. for some c, d, e, f,

$$G(s) = \frac{c - ds}{e - fs}. \tag{B4}$$

Therefore, the generating functions f_i are fractional-linear. It is readily verified that the functional composition of two fractional-linear functions is also fractional-linear. By induction, then, so is the composition of $n - 1$ fractional-linear functions, as in Eq. B2. Therefore, F_n is fractional-linear and the total number of E_n^*s has a semigeometric distribution, i.e. for some $A, B \geq 0$,

$$P_K =: Pr(K \text{ ions enter the cell}) = AB^{K-1}, \quad K \geq 1, \tag{B5}$$

where $Pr(H)$ denotes the probability of event H.

A quantum bump is produced if at least one ion enters the cell, which happens with probability

$$QE_A = 1 - P_0 = \sum_{K=1}^{\infty} P_K = \frac{A}{1 - B}. \tag{B6}$$

The probability that K ions enter the cell during a quantum bump is the conditional probability

$$P_{K|K\geq 1} =: \frac{A}{QE_A} B^{K-1} = (1 - B)B^{K-1}. \tag{B7}$$

Let Q be the mean charge carried by an E_n^*. Then, the mean quantum bump charge is

$$m_{L,A} =: \sum_{K=1}^{\infty} KQP_{K|K\geq 1} = \frac{Q}{1-B}. \tag{B8}$$

Therefore,

$$P_{K|K\geq 1} = \frac{Q}{m_{L,A}}\left[\left(1-\frac{Q}{m_{L,A}}\right)^{-m_{L,A}/Q}\right]^{-[(K-1)Q/m_{L,A}]}. \tag{B9}$$

In dark-adapted photoreceptors, the mean light-induced quantum bump charge is $\sim 10^9$ times the charge of a single ion. Therefore, to an excellent approximation, the quantum bump charge $(K-1)\,Q$ may be treated as a continuous variable x, the quantity in large brackets in Eq. B9 may be replaced by its limiting value as $Q/m_{L,A}$ approaches 0, exp(1), and the unconditional probability density for the charge output of Scheme A is

$$V_A(x) = (1-QE_A)\delta_0(x) + \frac{QE_A}{m_{L,A}}\exp\left(-\frac{x}{m_{L,A}}\right), \tag{B10}$$

where $V_{liqb,A}(x) =: (1/m_{L,A})\exp(-x/m_{L,A})$ is the exponential probability density for light-induced quantum bump charge.

The response charge probability distribution for scheme A. Substitution of $V_{liqb,A}$ and QE_A for their analogs in Eq. A1 yields the probability density for the charge of a purely light-induced response, where the resulting expression involves gamma functions (Ross, 1972, pp. 113–114)

$$\gamma\left(k,\frac{1}{m_{L,A}}\right)(x) =: \left(\frac{1}{m_{L,A}}\right)\left(\frac{x}{m_{L,A}}\right)^{k-1}\exp\left(-\frac{x}{m_{L,A}}\right) = \left(\frac{1}{m_{L,A}}\exp\left(-\frac{x}{m_{L,A}}\right)\right)^{*k}. \tag{B11}$$

Integration yields the corresponding cumulative charge distribution,

$$V_{\lambda_{li},A}^{cum}(x) = 1-\left(\exp\left(-\frac{x}{m_{L,A}}\right)\right)\sum_{r=0}^{\infty}\left(\frac{x}{m_{L,A}}\right)^r\left[1-e^{-\lambda(QE_A)}\sum_{k=0}^{r}\frac{[\lambda(QE_A)]^k}{k!}\right], \tag{B12}$$

where we have ordered the summations as shown for convenient numerical evaluation.

The scope of the scheme A activation and inactivation reaction mechanisms. Many types of molecular activation and inactivation mechanisms are consistent with Scheme A. The simplest are those of the Borsellino-Fuortes model (1968), where in every stage, both activation and inactivation occur as single chemical reactions with exponentially distributed waiting times (rates λ and μ in their notation). This implies (Ross, 1972, pp. 114–115) that our p_i equals their $\lambda/(\lambda+\mu)$ for all i. More generally, both activation and inactivation in Scheme A may involve multiple reactions and processes (e.g., diffusion) of arbitrary complexity, as long as an active enzyme molecule E_i^* always returns to the same reference state and biochemical environment before activating a molecule E_{i+1} in the next stage.

APPENDIX C

Light-induced Quantum Bump Charge and Response Charge Probability Distributions for Scheme B

Scheme B is described in Results. Here we show that its charge output has a three-parameter probability distribution that includes (*a*) a finite probability $1 - QE_B$ at zero charge (cascade failure), and (*b*) above zero charge, a light-induced quantum bump charge distribution that either decreases monotonically or exhibits a single peak. We also derive the cumulative charge distribution for a purely light-induced response.

The light-induced quantum bump charge distribution for scheme B. Continuing from the exposition in Results and using the results of Appendix B, we write the respective probability densities for the charge outputs of the M_1^* and M_2^* cascades as

$$V_{M_1^*}(x) = (f_{M_1^*})\delta_0(x) + \frac{(1 - f_{M_1^*})}{m_{M_1^*}} \exp\left(-\frac{x}{m_{M_1^*}}\right) \text{ and} \tag{C1}$$

$$V_{M_2^*}(x) = (f_{M_2^*})\delta_0(x) + \frac{(1 - f_{M_2^*})}{m_{M_2^*}} \exp\left(-\frac{x}{m_{M_2^*}}\right). \tag{C2}$$

The four parameters $f_{M_1^*}$, $f_{M_2^*}$, $m_{M_1^*}$ and $m_{M_2^*}$ are not independent, inasmuch as they are in part jointly determined by the gain production mechanisms after stage 1. To reveal their mutual dependence, we will use the fact that a cascade initiated by an E_2^* (to be called an "E_2^* cascade" and labeled a "subcascade" within Scheme B) has the gain production properties of a Scheme A cascade and therefore has some probability $f_{E_2^*}$ of failing to yield any charge output and probability $1 - f_{E_2^*}$ of yielding an exponentially distributed charge output with some mean $m_{E_2^*}$ (Appendix B). We will also apply the terms successful, effective, and their natural correlates to molecules, cascades, and subcascades as in the following examples. If the M_1^* cascade yields some (nonzero) charge output, it is successful (does not fail) and M_1^* is an effective molecule (it stimulates some charge output). By distinction, M_1^* is successful if it yields at least one E_2^* before becoming inactivated. M_1^* will be successful and yet ineffective if it yields one or more E_2^*s but none of the resulting E_2^* cascades succeeds in yielding any charge output (none of the E_2^*s is effective). Thus, an effective M_1^* implies at least one effective E_2^*.

Now, let $p_{M_1^*,k} =: (p_{M_1^*})^k(1 - p_{M_1^*})$ be the geometric probability that M_1^* produces exactly k E_2^*s before becoming inactivated (see Eq. B3) and let $p_{M_2^*,k} =: (p_{M_2^*})^k(1 - p_{M_2^*})$ be the analogous probability for M_2^*. Then,

$$\begin{aligned} f_{M_1^*} &= Pr(M_1^* \text{ is ineffective}) \\ &= \sum_{k=0}^{\infty} Pr(M_1^* \text{ is ineffective} \mid M_1^* \text{ yields } k\ E_2^*s) Pr(M_1^* \text{ yields } k\ E_2^*s) \\ &= \sum_{k=0}^{\infty} Pr(M_1^* \text{ yields } k\ E_2^*s) Pr(k\ E_2^* \text{ cascades fail}) = \sum_{k=0}^{\infty} (p_{M_1^*,k})(f_{E_2^*})^k \\ &= \frac{(1 - p_{M_1^*})}{1 - (p_{M_1^*})(f_{E_2^*})}. \end{aligned} \tag{C3}$$

Also, the mean charge output from the M_1^* cascade (counting both failures and successes of the M_1^* cascade) is $(1 - f_{M_1^*})(m_{M_1^*})$, which must equal the product of the mean number of E_2^* s produced by M_1^*, $[p_{M_1^*}/(1 - p_{M_1^*})]$ (see Ross, 1972, p. 48 and Chapter 3), and the mean charge output of an E_2^* cascade (including both cascade successes and failures), $(1 - f_{E_2^*})(m_{E_2^*})$. Thus,

$$(1 - f_{M_1^*})m_{M_1^*} = \left(\frac{p_{M_1^*}}{1 - p_{M_1^*}}\right)(1 + f_{E_2^*})m_{E_2^*}.$$

Calculating $1 - f_{M_1^*}$ from C3, substituting into C4 and rearranging yields $m_{M_1^*}[(1 - p_{M_1^*})/(1 - (p_{M_1^*})(f_{E_2^*}))] = m_{E_2^*}$, or, substituting again from C3, $(m_{M_1^*})(f_{M_1^*}) = m_{E_2^*}$. Similarly, $(m_{M_2^*})(f_{M_2^*}) = m_{E_2^*}$, and therefore

$$(f_{M_1^*})(m_{M_1^*}) = (f_{M_2^*})(m_{M_2^*}), \tag{C5}$$

which shows that only three of the four parameters in Eqs. C1 and C2 are independent.

Given that the sum of the charge outputs of the independent M_1^* and M_2^* cascades equals the charge output of Scheme B, the latter has a probability density $V_B(x)$ that must be the convolution

$$V_B(x) = ((V_{M_1^*}) * (V_{M_2^*}))(x) =: \int_{t=0}^{x} V_{M_1^*}(t)V_{M_2^*}(x - t)dt$$

$$= \begin{cases} [(f_{M_1^*})(f_{M_2^*})\delta_0(x)] + \left[(f_{M_2^*})\dfrac{(1 - f_{M_1^*})}{m_{M_1^*}}\exp\left(-\dfrac{x}{m_{M_1^*}}\right)\right] \\ + \left[(f_{M_1^*})\dfrac{(1 - f_{M_2^*})}{m_{M_2^*}}\exp\left(-\dfrac{x}{m_{M_2^*}}\right)\right] \\ + \left[(1 - f_{M_1^*})(1 - f_{M_2^*})\left(\dfrac{1}{m_{M_2^*} - m_{M_1^*}}\right)\right. \\ \left.\left(\left(-\dfrac{x}{m_{M_2^*}}\right) - \exp\left(-\dfrac{x}{m_{M_1^*}}\right)\right)\right]\exp,\ m_{M_1^*} \neq m_{M_2^*}, \\ [(f)^2\delta_0(x)] + \left[2\dfrac{(f)(1 - f)}{m}\exp\left(-\dfrac{x}{m}\right)\right] \\ + \left[\dfrac{(1 - f)^2}{m}\left(\dfrac{x}{m}\right)\exp\left(-\dfrac{x}{m}\right)\right],\ m_{M_1^*} = m_{M_2^*} =: m, \end{cases} \tag{C6}$$

where it is understood that C5 holds, $f_{M_1^*} = f_{M_2^*} =: f$ when $m_{M_1^*} = m_{M_2^*} =: m$, and $0 \leq f_{M_1^*}, f_{M_2^*} < 1$. The coefficient of $\delta_0(x)$ in C6 equals $1 - QE_B$, where QE_B is the quantum efficiency of Scheme B given that rhodopsin is photoactivated to M_1^*. The Scheme B probability density for light-induced quantum bump charge, $V_{liqb,B}(x)$, equals $1/QE_B$ times the sum of the three (two) right-most square-bracketed terms in the top (bottom) expression of C6. The mean light-induced quantum bump charge, $m_{L,B}$, equals the total mean charge output of the M_1^* and M_2^* cascades divided by the

probability of non-zero total output (see Ross, 1972, Chapter 3), or

$$m_{L,B} = \frac{(1 - f_{M_1^*})m_{M_1^*} + (1 - f_{M_2^*})m_{M_2^*}}{QE_B}. \tag{C7}$$

The shape of the light-induced quantum bump charge distribution for scheme B. It is convenient to define $\alpha =: \max [1/m_{M_1^*}, 1/m_{M_2^*}]$, $\beta =: \min [1/m_{M_1^*}, 1/m_{M_2^*}]$, $M_\alpha^* =: M_1^*$ if $\alpha = 1/m_{M_1^*}$ and $=: M_2^*$ otherwise, $M_\beta^* =: M_2^*$ if $\beta = 1/m_{M_2^*}$ and $=: M_1^*$ otherwise, $q_\alpha =: 1 - f_{M_\alpha^*}$, $q_\beta =: 1 - f_{M_\beta^*}$, $v =: (q_\alpha)[1 + (q_\beta)\alpha/(\beta - \alpha)]$, $w =: (q_\beta)[1 + (q_\alpha)\beta/(\alpha - \beta)]$, and $u =: 1 - (v + w)$ (one may also note $u = 1 - QE_B = (1 - q_\alpha)(1 - q_\beta) = 1 - (\alpha/\beta)(1 - q_\beta)^2$), and to consider only the case $\alpha \neq \beta$ and hence $\alpha > \beta$, whereupon

$$V_B(x) = u\delta_0(x) + v\alpha e^{-\alpha x} + w\beta e^{-\beta x}, \tag{C8}$$

$$V_{liqb,B}(x) = \frac{1}{1 - u}(v\alpha e^{-\alpha x} + w\beta e^{-\beta x}) \text{ and} \tag{C9}$$

$$m_{L,B} = \frac{1}{1 - u}\left(\frac{v}{\alpha} + \frac{w}{\beta}\right). \tag{C10}$$

In view of C5, $q_\beta = 1 - (\beta/\alpha)(1 - q_\alpha)$, so $v = (q_\alpha)^2[\beta/(\beta - \alpha)]$; also, $w = (q_\beta)^2[\alpha/(\alpha - \beta)]$, whereupon $V_{liqb,B}(x) = (w\beta/QE_B)[e^{-\beta x} - (q_\alpha/q_\beta)^2 e^{-\alpha x}]$. Equating the first derivative of this last expression to zero yields $e^{(\alpha-\beta)x} = (\alpha/\beta)/(q_\alpha/q_\beta)^2$, which, in view of C5, equals $((1 - q_\alpha)/(1 - q_\beta))(q_\alpha/q_\beta)^2$. Because $e^{(\alpha-\beta)x}$ increases monotonically with x from the value 1 at $x = 0$, and because $V_{liqb,B}(x)$ is a probability density and must therefore approach 0 as $x \to \infty$, $V_{liqb,B}(x)$ has a single extremum and this extremum is a maximum. If $[(1 - q_\alpha)/(1 - q_\beta)](q_\alpha/q_\beta)^2 \leq 1$ (e.g., for q_α slightly above zero) the maximum is at $x = 0$. If $[(1 - q_\alpha)/(1 - q_\beta)](q_\alpha/q_\beta)^2 > 1$ (e.g., for both q_α and q_β slightly < 1), the maximum is at some value $x > 0$. Thus, $V_{liqb,B}(x)$ either decreases monotonically with x or has a single peak.

The response charge probability distribution for scheme B. We have

$$(V_{liqb,B})^{*k}(x) = \sum_{j=0}^{k} \binom{k}{j} \left(\frac{v}{1 - u}\right)^j \left(\frac{w}{1 - u}\right)^{k-j} [\gamma(j, \alpha) * \gamma(k - j, \beta)](x), \tag{C11}$$

where $\gamma(\,)$ is defined in Appendix B. To evaluate $[\gamma(n, \alpha) * \gamma(m, \beta)](x)$, where n, $m \geq 1$ are integers, we use the characteristic function $\hat{\xi}(t) =: \int_{-\infty}^{\infty} \xi(x)e^{itx}\,dx$ (a Fourier transform) of a probability density $\xi(x)$ and its properties (Feller, 1971, p. 498). Thus,

$$[\gamma(n, \alpha) * \gamma(m, \beta)]\hat{}(t) = \left(\frac{\alpha}{\alpha - it}\right)^n \left(\frac{\beta}{\beta - it}\right)^m := g(t). \tag{C12}$$

To invert Eq. C12, we take partial fractions (see Lentner and Buehler, 1964), letting $\omega =: i/\alpha$ and $\zeta =: i/\beta$ and expanding $g(t)$ as

$$g(t) = \sum_{j=1}^{n} b_j(1 - \omega t)^{-j} + \sum_{k=1}^{m} c_k(1 - \zeta t)^{-k}. \tag{C13}$$

Using this expansion to express $(1/(1 - \zeta t))^m$, differentiating the expression with respect to t and evaluating the derivative at $t = 1/\omega$ yields the coefficients b_j. The coefficients c_k are obtained similarly. An inverse Fourier transform then yields the desired expression for the convolution of gammas in C11. The probability density for the charge of a purely light-induced response follows per A1 [with $\lambda_{li} = \lambda(QE_B) = \lambda(1 - u)$]. Then, letting $\xi =: \lambda v$ and $\eta =: \lambda w$, integration yields the corresponding cumulative distribution,

$$V^{cum}_{\lambda_{li},B}(x) = 1 - e^{-\xi-\eta}$$
$$\times \left[e^{-\alpha x} \sum_{r=0}^{\infty} \frac{(\alpha x)^r}{r!} \left[\frac{\xi^{r+1}}{(r+1)!} + \sum_{k=r+2}^{\infty} \frac{1}{k!} \left\{ \xi^k + \sum_{j=r+1}^{k-1} \binom{k}{j} \xi^j \eta^{k-j} \left(-\frac{\alpha}{\beta} \right)^j \frac{C_{r,j,k}}{\left(1 - \frac{\alpha}{\beta}\right)^k} \right\} \right] \right. \quad \text{(C14)}$$
$$\left. + e^{-\beta x} \sum_{r=0}^{\infty} \frac{(\beta x)^r}{r!} \left[\frac{\eta^{r+1}}{(r+1)!} + \sum_{k=r+2}^{\infty} \frac{1}{k!} \left\{ \eta^k + \sum_{j=1}^{k-r-1} \binom{k}{j} \xi^j \eta^{k-j} \left(-\frac{\beta}{\alpha} \right)^{k-j} \frac{D_{r,j,k}}{\left(1 - \frac{\beta}{\alpha}\right)^k} \right\} \right] \right],$$

with

$$C_{r,j,k} =: \sum_{i=r}^{j-1} \left(1 - \frac{\beta}{\alpha}\right)^{i+1} \binom{k-i-2}{k-j-1} \quad \text{and}$$
$$D_{r,j,k} =: \sum_{i=r}^{k-j-1} \left(1 - \frac{\alpha}{\beta}\right)^{i+1} \binom{k-i-2}{j-1}. \quad \text{(C15)}$$

Note that the working assumption $\alpha > \beta$ implies $q_\beta > 1 - (\beta/\alpha)$ and $0 < q_\alpha < q_\beta < 1$ (one may also note $QE_B > 1 - (\beta/\alpha)$), whereupon it is seen that the constraints $0 < (\alpha - \beta)/\alpha < w < \alpha/(\alpha - \beta)$ and $\beta/(\beta - \alpha) < v < 0$ apply to $\xi =: \lambda v$ and $\eta =: \lambda w$ in C14.

APPENDIX D

The Influence of the First Stage of Amplification on the Size Variability of Light-induced Quantum Bumps

Here we explore how the first stage of cascade amplification influences the variability of light-induced quantum bump charge. First, we derive a simple formula (Eq. D3) for the peakedness of the charge distribution, quantified through the coefficient of variation (standard deviation/mean). This formula is valid for a very broad class of cascade models that extend far beyond Schemes A and B. The formula shows that the peakedness is nearly determined by the fewest initial stages that on average contribute a high "effective" cumulative gain (defined below) to a quantum bump. We next exemplify the utility of this formula through its application to Scheme B. Finally, we outline why not just the peakedness, but practically the entire charge distribution, is nearly determined by the first stage of the cascade (e.g., G protein activation) if the effective gain from this stage is high, regardless of the nature of the amplification

processes after this stage. Related discussion can be found in Grzywacz and Hillman (1985).

The peakedness of the light-induced quantum bump charge distribution for cascade models. We consider any cascade for which the charge of a light-induced quantum bump equals the sum of independent, identically distributed charge outputs from one or more successful subcascades initiated respectively by E_j^*s in any stage $j = 2, 3, 4, \ldots,$ or $n - 1$ ("effective" E_j^*s; see foregoing appendices for the definition of terms, especially after Eq. C2). For some one of these stages j, let N be the number of effective E_j^*s, X the charge output of a successful E_j^*cascade, and Y the charge of a quantum bump, i.e., the charge output when the cascade as a whole is successful, which implies $N \geq 1$. Then, denoting the conditional mean and variance of N given that $N \geq 1$ by $E[N|N \geq 1]$ and $\mathrm{Var}[N|N \geq 1]$, respectively, we have

$$E[Y] = E[N|N \geq 1]E[X], \tag{D1}$$

$$\mathrm{Var}[Y] = \mathrm{Var}[N|N \geq 1](E[X])^2 + E[N|N \geq 1]\,\mathrm{Var}[X], \tag{D2}$$

(Ross, 1972, p. 71), and, therefore,

$$\frac{\mathrm{Var}[Y]}{(E[Y])^2} = \frac{\mathrm{Var}[N|N \geq 1]}{(E[N|N \geq 1])^2} + \frac{1}{E[N|N \geq 1]}\frac{\mathrm{Var}[X]}{(E[X])^2}. \tag{D3}$$

$E[N|N \geq 1]$ is the mean of a quantity that may be called the "effective cumulative quantum bump gain through stage $j - 1$." Eq. D3 shows that the light-induced quantum bump charge distribution is always broader than the distribution of the effective cumulative quantum bump gain, but approaches this distribution in peakedness as the mean effective cumulative gain grows. Of special interest is high effective gain from stage 1 ($j = 2$), in which case the peakedness of the quantum bump charge distribution nearly equals the peakedness of the distribution of, e.g., the number of effective G proteins.

The peakedness of the light-induced quantum bump charge distribution for scheme B. Using the identities

$$E[N|N \geq 1] = \frac{E[N]}{1 - Pr(N = 0)} \quad \text{and} \tag{D4}$$

$$\mathrm{Var}[N|N \geq 1] = \frac{\mathrm{Var}[N]}{1 - Pr(N = 0)} + \frac{(E[N])^2}{1 - Pr(N = 0)} - \frac{(E[N])^2}{[1 - Pr(N = 0)]^2}, \tag{D5}$$

we apply D3 to Scheme B with $j = 2$, recalling from Appendix C that M_α^* *and* M_β^* yield independent, geometrically distributed numbers of E_2^*s and that the charge stimulated by an effective E_2^* is exponentially distributed, which implies $\mathrm{Var}[X]/(E[X])^2 = 1$ (Ross, 1972, p. 49). Using a composition of generating functions, as in B1–B4, one may demonstrate the intuitively plausible fact that the respective numbers of effective E_2^*s produced by M_α^* and M_β^* (to be called N_α and N_β, respectively) are also geometrically distributed. In fact, one sees from the definitions of q_α and q_β in Appendix C that $Pr(N_\alpha = j) = (1 - q_\alpha)(q_\alpha)^j$, and similarly for N_β. Therefore, $E[N_\alpha] = q_\alpha/(1 - q_\alpha)$, $E[N_\beta] = q_\beta/(1 - q_\beta)$, $\mathrm{Var}[N_\alpha] = q_\alpha/(1 - q_\alpha)^2$, and $\mathrm{Var}[N_\beta] = q_\beta/(1 - q_\beta)^2$. Also, $E[N] = E[N_\alpha] + E[N_\beta]$, and, from the independence of N_α and N_β, $\mathrm{Var}[N] =$

$\mathrm{Var}[N_\alpha] + \mathrm{Var}[N_\beta]$ (Ross, 1972, pp. 39–42,71). We also recall from Appendix C that $1 - \Pr(N = 0) = \mathrm{QE_B} = 1 - (1 - q_\alpha)(1 - q_\beta)$. Substitution into D3 yields, after algebraic manipulations,

$$\frac{\mathrm{Var}[Y]}{(E[Y])^2} = 1 - \frac{2q_\alpha q_\beta \dfrac{q_\beta(1 - q_\alpha)}{q_\alpha(1 - q_\beta)}}{\left(1 + \dfrac{q_\beta(1 - q_\alpha)}{q_\alpha(1 - q_\beta)}\right)^2}. \tag{D6}$$

Letting $r = q_\beta(1 - q_\alpha)/[q_\alpha(1 - q_\beta)]$, one sees that D6 attains its minimum value of ½ (most peaked quantum bump charge distribution) when $q_\alpha q_\beta$ and $r/(1 + r)^2$ are simultaneously maximum, which occurs for $q_\alpha \to q_\beta \to 1$. This case represents the limit of equivalent and indefinitely-high-gain-producing M^*_α and M^*_β, and implies a gamma probability density for quantum bump charge x, $(\xi x)(\xi)\exp(-\xi x)$, for some indefinitely small, positive ξ. D6 attains its maximum value of 1 (least peaked charge distribution) for one of q_α or $q_\beta \to 0$. This case represents the limit of M^*_α producing indefinitely low gain and an exponential quantum bump charge distribution (Scheme B reduces to Scheme A). In general, for equivalent M^*_α and M^*_β ($q_\alpha \to q_\beta := q$), D6 reduces to the simpler form

$$\frac{\mathrm{Var}[Y]}{(E[Y])^2} = 1 - \frac{q^2}{2}, \tag{D7}$$

and corresponds to a mean effective first-stage gain of $E[N|N \geq 1] = [1/(1 - q)^2]$ $2q/(1 - q)$.

The influence of the first stage of amplification on the form of the light-induced quantum bump charge distribution. We now consider all models with a first stage consisting of a sequence of active states (M^*_α, M^*_β , M^*_γ, . . .), each of which produces a geometrically distributed amount of effective gain (N_α, N_β, N_γ, . . .), and where we again let X take on any distribution.

Our main objective is to explain at a nondetailed level that, regardless of the distribution of X, as the average effective gains $E[N_\alpha]$, $E[N_\beta]$, $E[N_\gamma]$, . . . become large, the light-induced quantum bump charge distribution approaches a convolution of exponentials, which is also the limiting form of the distribution for the total effective first-stage gain, $N_\alpha + N_\beta + N_\gamma + \cdots$ (a single exponential if there is only one active state, M^*_α). We also comment on the relevance of this result to practical transduction cascade models, in which the effective first-stage gain (e.g., number of activated G proteins) may be only moderately large (≈ 10).

First, we consider $\Sigma_{i=1}^{N_\alpha} X_i/E[N_\alpha]$ (defined to be 0 for $N_\alpha = 0$) and rewrite it as $(N_\alpha/E[N_\alpha])\cdot(\Sigma_{i=1}^{N_\alpha} X_i/N_\alpha)$. As $E[N_\alpha]$ becomes large, the left term becomes exponentially distributed with mean 1 (Feller, 1971, p. 2) and N_α usually takes on large values, for which the right term approaches $E[X]$ by the strong law of large numbers (Feller, 1971, p. 238). Therefore, the product of the two terms becomes exponentially distributed with mean $E[X]$. Equivalently, the distribution of the charge contribution stimulated by M^*_α becomes an exponential, which is also the limiting distribution form for the effective gain produced by M^*_α.

Generalizing, as the average effective gains $E[N_\alpha]$, $E[N_\beta]$, $E[N_\gamma]$, . . . become large,

the respective distributions for the charge contributions stimulated by M^*_α, M^*_β, M^*_γ, . . . become exponentials, like the distributions of the corresponding effective gains. Therefore, the distribution for the sum of the charge contributions approaches a convolution of exponentials, as does the distribution for the total effective first-stage gain. Under these conditions, the cascade almost always results in a quantum bump, so the quantum bump charge distribution is practically the same as the convolution of exponentials.

What if the average total effective first-stage gain is only moderately large, e.g., near 10? This would suggest, for example, average effective gains near 5 for the two active metarhodopsin states of Scheme B. Such numbers are not very large in the usual sense of the limits invoked here, but are large enough to suggest some resemblance of the quantum bump charge distribution to a convolution of exponentials for a wide variety of possible transduction processes after the first stage (e.g., see Fig. 5).

APPENDIX E

Details for Tables

Details for Table I. Here we discuss the definitions and estimation of the statistical parameters of Table I (see Materials and Methods, Results, Appendix A, and Ross, 1972, Chapter 3 for background). We also provide additional experimental notes on Cell 4 and on the relationship between Cell 2A and Cell 2B.

n is the number of consecutive flashes that yielded stable data. An observed, or measured response signifies that at least one quantum bump (light-induced or spontaneous) beginning in the response period was detected. $n_{R<}$ and $n_{R\geq}$ are respectively the number of observed responses with charge $<$ and $\geq C_{min}$. Thus, $n - n_{R<} - n_{R\geq}$ is the number of nonresponses. $n_{S<}$ and $n_{S\geq}$ are respectively the total number of detected spontaneous quantum bumps with charge $<$ and $\geq C_{min}$ beginning in the n spontaneous quantum bump observation periods. $p_{OBS} =: Pr$(a flash is followed by an observed response), which is estimated (see Bevington, 1969, pp. 53, 78) as $p_{OBS} = ((n_{R<} + n_{R\geq})/n) \pm \sqrt{p_{OBS}(1 - p_{OBS})n}/n$. Similarly, $p_S =: Pr$(a flash is followed by one or more spontaneous quantum bumps that begin in the response period) $= [(n_{S<} + n_{S\geq})/n] \times (L_{RP}/L_{SQBOP}) \pm \sqrt{p_S(1 - p_S)n}/n$, where L_{RP} and L_{SQBOP} are respectively the lengths of the response period and spontaneous quantum bump observation period (ms). $p_L =: Pr$(a flash is followed by at least one light-induced quantum bump beginning in the response period) $= (p_{OBS} - p_S)/(1 - p_S)$. $w_L =: Pr$(an observed response comprises only light-induced quantum bumps) $= p_L(1 - p_S)/p_{OBS}$. $w_S =: Pr$(an observed response comprises only spontaneous quantum bumps) $= p_S(1 - p_L)/p_{OBS}$. $w_{LS} =: Pr$(an observed response comprises at least one light-induced quantum bump and at least one spontaneous quantum bump) $= p_S p_L/p_{OBS}$. From the Poisson distribution (see Appendix A), the mean numbers of light-induced and spontaneous quantum bumps beginning in the response period are $\lambda_{li} = -\ln(1 - p_L)$ and $\lambda_s = -\ln(1 - p_S) \approx p_S$ for $p_S \ll 1$. $\lambda_{li,c} =:$ the conditional mean number of light-induced quantum bumps in an observed response given that the response comprises at least one light-induced quantum bump $= \lambda_{li}/p_L$. $p_{mult} =: Pr$(an observed response that comprises at least one

light-induced quantum bump comprises at least two light-induced quantum bumps). By the Poisson distribution, $p_{\text{mult}} = (1 - e^{-\lambda_{\text{li}}} - \lambda_{\text{li}}e^{-\lambda_{\text{li}}})/(1 - e^{-\lambda_{\text{li}}})$. $m_{\text{OBS}} =:$ the average charge of the $n_{\text{R}<} + n_{\text{R}\geq}$ observed responses, expressed ± its standard error. $m_{\text{S}} =:$ the average charge of the $n_{\text{S}<} + n_{\text{S}\geq}$ spontaneous quantum bumps. $m_{\text{L}} =:$ the average light-induced quantum bump charge, estimated as $(M_{\text{OBS}}p_{\text{OBS}} - p_{\text{S}}m_{\text{S}})/\lambda_{\text{li}}$.

Additional notes on experiments are as follows. Cell 2 was left in the dark ~8 min after flash series A (Cell 2A), then stimualted at ~3.5 times lower flash intensity for flash series B (Cell 2B). In Cell 4, the spontaneous quantum bump rate exhibited statistically significant short-term fluctuation. So few spontaneous quantum bumps occurred in that cell, however, that the fluctuation had negligible impact on the analysis of the response charge distribution (see Materials and Methods).

Details for Table III. Notes on table quantities, which are defined in Results and Appendices A–D, are as follows. For Scheme A, the standard deviation/mean for quantum bump charge (last row) always equals 1 because the charge distribution is exponential (Appendix B; Ross, 1972, p. 49). The quantum efficiency parameter QE_{A} cannot be estimated from the data (only $\lambda_{\text{li,A}} =: \lambda(\text{QE}_{\text{A}})$ can be estimated; see Eq. B12).

The Scheme B parameters were computed according to (see Appendix C): $m_{M_1^*} = \min(1/\alpha, 1/\beta)$; $m_{M_2^*} = \max(1/\alpha, 1/\beta)$; $1 - f_{M_2^*} = q_\beta = (Z_1 + \sqrt{(Z_1)^2 - Z_2Z_3})/Z_2$, where $Z_1 =: (\alpha/\beta) - 1$, $Z_2 =: (\alpha/\beta) + (\xi/\eta)$, and $Z_3 =: (\alpha/\beta) + (\beta/\alpha) - 2$; $1 - f_{M_1^*}^* = q_\alpha = 1 - (\alpha/\beta)(1 - q_\beta)$; $\text{QE}_{\text{B}} = q_\alpha + q_\beta - q_\alpha q_\beta$; $\lambda_{\text{li,B}} =: \lambda(\text{QE}_{\text{B}}) = \xi + \eta$; $m_{\text{L,B}} = [(q_\alpha/\alpha) + (q_\beta/\beta)]/\text{QE}_{\text{B}}$; $m_{E_2^*} = (f_1^*)(m_{M_1^*}) = (f_{M_2^*})(m_{M_2^*})$. The standard deviation/mean for quantum bump charge was calculated according to Eq. D6. The values of the quantum efficiency parameter QE_{B} are very close to 1 and therefore reasonable (Fein and Szuts, 1982). The true values of many of these quantities are highly uncertain, inasmuch as values were found for the independent parameters that, although far from the values listed, yielded a fit almost as good as the best fit.

For Cell 1, Scheme B fits best when ξ takes on its maximum allowed value of 0 (Appendix C, last paragraph). This value implies that one of the active metarhodopsin states (here, arbitrarily chosen as M_1^*) is completely ineffective and thus Scheme B reduces to Scheme A. Thus, $m_{M_1^*}$ is arbitrary, the other parameter values align with Scheme A, and some of them (e.g., QE_{B}) cannot be estimated from the data.

Details for Table IV. By the procedures described in Materials and Methods, X^2_{min} was found in all cases except Scheme B, Cells 2A and 2B, for which calculations became numerically unstable in some parameter regions. For these two experiments, the X^2_{min} values listed are the smallest accurate values found. The true values are at least as small, and correspond to significance probabilities at least as large as those listed.

The number of free model parameters d equals: 2 for Scheme A, and; 4 for Scheme B, except for Cell 1, where Scheme B reduced to Scheme A (see Details for Table III) and thus 2 of the 4 Scheme B parameters could not be meaningfully varied around best-fit values as can in general be done at X^2_{min}. The correct χ^2 distribution in this case has somewhere between 4 and 6 degrees of freedom. Hence, the range given in the table for the significance probability of Scheme B, Cell 1. To appreciate the smallness of this probability (P), consider that for a true model, the significance probabilities for a set of N independent experiments should be about uniformly

distributed between 0 and 1. Thus, Pr(one or more of N significance probabilities is $\leq P$) = 1-Pr(all N significance probabilities are $> P$) = $1 - (1 - P)^N$, which here ($N = 5$) is approximately between 0.03 and 0.13 (see Results).

The authors would like to thank Richard M. Dudley for contributing most of the mathematics of Appendices A, B, and C, the statistical methodology described in Materials and Methods, and the chi-square minimization results of Tables II through IV, as well as for many helpful discussions; Ward Whitt for pointing out the mathematics discussed in the last section of Appendix D; Daniel Jeske for helpful discussions; Chris Miller, Jeff Haul, and David Tank for the use of computing facilities; and Alfredo Kirkwood for reviewing the manuscript.

This work was supported by grant EY01496 to J. Lisman.

Original version received 29 June 1993 and accepted version received 27 September 1993.

REFERENCES

Adolph, A. 1964. Spontaneous slow potential fluctuations in the *Limulus* photoreceptor. *Journal of General Physiology.* 48:297–322.

Bacigalupo, J., K. Chinn, and J. E. Lisman. 1986. Ion channels activated by light in *Limulus* ventral photoreceptors. *Journal of General Physiology.* 87:73–89.

Bevington, P. R. 1969. Data Reduction and Error Analysis for the Physical Sciences. McGraw-Hill Book Company, New York.

Bickel, P. J., and K. A. Doksum. 1977. Mathematical Statistics. Holden-Day, San Francisco.

Borsellino, A., and M. G. F. Fuortes. 1968. Responses to single photons in visual cells of *Limulus*. *Journal of Physiology.* 196:507–539.

Colquhoun, D., and A. G. Hawkes. 1984. The principles of the stochastic interpretation of ion-channel mechanisms. *In:* Single-Channel Recording. B. Sakmann and E. Neher, editors. Plenum Publishing Corp., New York. 135–174.

Cone, R. A. 1973. The internal transmitter model for visual excitation: some quantitative implications. *In* Biochemistry and Physiology of Visual Pigments. H. Langer, editor. Springer-Verlag, Berlin. 275–282.

Darling, D. A. 1957. The Kolmogorov-Smirnov, Cramer-von Mises tests. *Annals of Mathematical Statistics.* 28:823–838.

Fein, A., and E. Z. Szuts. 1982. Photoreceptors: Their Role in Vision. Cambridge University Press, Cambridge.

Feller, W. 1968. An Introduction to Probability Theory and Its Applications. Vol. 1. John Wiley and Sons, Inc., New York.

Feller, W. 1971. An Introduction to Probability Theory and Its Applications. Vol. 2. John Wiley and Sons, Inc., New York.

Fuortes, M. G. F., and A. L. Hodgkin. 1964. Changes in time scale and sensitivity in the ommatidia of *Limulus*. *Journal of Physiology,* 172:239–263.

Fuortes, M. G. F., and S. Yeandle. 1964. Probability of occurrence of discrete potential waves in the eye of *Limulus*. *Journal of General Physiology.* 47:443–463.

Goldring, M. A. 1980. Quantum bumps in *Limulus* ventral photoreceptors have complex shapes. *Biophysical Journal.* 35:2063.

Goldring, M. A., and J. E. Lisman. 1983. Single photon transduction in *Limulus* photoreceptors and the Borsellino-Fuortes model. *IEEE Transactions on Systems, Man, and Cybernetics.* SMC. 13:727–731.

Grzywacz, N. M., and P. Hillman. 1985. Statistical test of linearity of photoreceptor transduction process: *Limulus* passes, others fail. *Proceedings of the National Academy of Sciences, USA.* 82:232–235.

Harris, T. E. 1963. The Theory of Branching Processes. Springer Verlag, Berlin.

Holt, R. J. 1986. Computation of gamma and beta tail probabilities. Technical Report, Mathematics Department, Massachusetts Institute of Technology, Cambridge, MA.

Howard, J. 1983. Variations in the voltage response to single quanta of light in the photoreceptors of *Locusta Migratoria. Biophysics of Structure and Mechanism.* 9:341–348.

Jagers, P. 1974. Galton-Watson processes in varying environments. *Journal of Applied Probability.* 11:174–178.

Kim, P. J., and R. I. Jennrich. 1973. Tables of the exact sampling distribution of the two-sample Kolmogorov-Smirnov criterion D_{mn}, $m \leq n$. *In* Selected Tables in Mathematical Statistics. Vol. 1. H. L. Harter and D. B. Owen, editors. Institute of Mathematical Statistics and the American Mathematical Society, Providence, RI.

Kirkwood, A., D. Weiner, and J. E. Lisman. 1989. An estimate of the number of G regulatory proteins activated per excited rhodopsin in living *Limulus* ventral photoreceptors. *Proceedings of the National Academy of Sciences, USA.* 86:3872–3876.

Kuhn, H., S. W. Hall, and U. Wilden. 1984. Light-induced binding of 48-kD protein to photoreceptor membranes is highly enhanced by phosphorylation of rhodopsin. *FEBS Letters* 176:473–478.

Lederhofer, R., J. Schnakenberg, and H. Stieve. 1991. Stochastic treatment of bump latency and temporal overlapping in *Limulus* ventral photoreceptors. *Zeitschrift fur Naturforschung.* 46c:291–304.

Lentner, M. M., and R. J. Buehler. 1964. Some inferences about gamma parameters with an application to a reliability problem. *Journal of the American Statistical Association.* 58:670.

Lillywhite, P. G. 1977. Single photon signals and transduction in an insect eye. *Journal of Comparative Physiology.* 122:189–200.

Lisman, J. 1985. The role of metarhodopsin in the generation of spontaneous quantum bumps in ultraviolet receptors of *Limulus* median eye. Evidence for reverse reactions into an active state. *Journal of General Physiology.* 85:171–187.

Lisman, J. E., and J. E. Brown. 1971. Two light-induced processes in the photoreceptor cells of *Limulus* ventral eye. *Journal of General Physiology.* 58:544–561.

Lisman, J. E., and J. E. Brown. 1975. Light-induced changes of sensitivity in *Limulus* ventral photoreceptors. *Journal of General Physiology.* 66:473–488.

Lisman, J., and M. Goldring. 1985. Early events in visual transduction in *Limulus* photoreceptors. *Neurosciences Research.* 2:(Suppl.)101–117.

Martinez, J. M., and R. Srebro. 1976. Calcium and the control of discrete wave latency in the ventral photoreceptor of *Limulus. Journal of Physiology.* 261:535–562.

Millecchia, R., and A. Mauro. 1969. The ventral photoreceptor cells of *Limulus.* III. A voltage clamp study. *Journal of General Physiology.* 54:331–351.

Ross, S. M. 1972. Introduction to Probability Models. Academic Press, New York.

Sitaramayya, A., and P. A. Liebman. 1983. Phosphorylation of rhodopsin and quenching of cyclic GMP phosphodiesterase by ATP at weak bleaches. *Journal of Biological Chemistry.* 358:13106–13109.

Smith, D. P., B. Shieh, and C. S. Zucker. 1990. Isolation and structure of an arrestin gene from *Drosophila. Proceedings of the National Academy of Sciences, USA.* 87:1005–1007.

Sokol, B. A., and R. Srebro. 1982. Evidence for coupling among *Limulus* ventral photoreceptors. *Investigative Ophthalmology and Visual Science.* 22(Suppl.):275.

Srebro, R., and M. Behbehani. 1972. The thermal origin of spontaneous activity in the *Limulus* photoreceptor. *Journal of Physiology.* 224:349–361.

Srebro, R., and S. Yeandle. 1970. Stochastic properties of discrete waves of the *Limulus* photoreceptor. *Journal of General Physiology.* 56:751–767.

Stadtman, E. R., and P. B. Chock. 1979. Advantages of enzyme cascades in the regulation of key metabolic processes. *In* The Neurosciences. F. O. Schmitt and F. G. Worden, editors. MIT Press, Cambridge, MA. 801–817.

Stern, J., K. Chinn, J. Bacigalupo, and J. E. Lisman. 1982. Distinct lobes of *Limulus* ventral photoreceptors. I. Functional and anatomical properties of lobes revealed by removal of glial cells. *Journal of General Physiology.* 85:157–169.

Stieve, H., and M. Bruns. 1983. Bump latency distribution and bump adaptation of *Limulus* ventral nerve photoreceptor in varied extracellular calcium concentrations. *Biophysics of Structure and Mechanism.* 9:329–339.

Stieve, H., H. Reuss, H. T. Hennig, and J. Klomfass. 1990. Single photon-evoked events of the ventral nerve photoreceptor cell of *Limulus*. Facilitation, adaptation and dependence on lowered external calcium. *Zeitschrift fur Naturforschung.* 46c:461–486.

Stryer, L. 1986. Cyclic GMP cascade of vision. *Annual Reviews of Neuroscience.* 9:87–119.

Tiedge, J. 1981. Deterministische und stochastische Modeltheorien zur Photorezeption des Pfeilschwanzkrebses *Limulus* polyphemus. PhD thesis. Rhein-Westf. Technischen Hochschule, Aachen, Germany.

Vandenberg, C. A., and M. Montal. 1984. Light-regulated biochemical events in invertebrate photoreceptors. II. Light-regulated phosphorylation of rhodopsin and phosphoinositides in squid photoreceptor membranes. *Biochemistry.* 23:2347–2352.

Wilden, U., S. W. Hall, and H. Kuhn. 1986. Phosphodiesterase activation by photoexcited rhodopsin is quenched when rhodopsin is phosphorylated and binds the intrinsic 48-KDa protein of rod outer segments. *Proceedings of the National Academy of Sciences, USA.* 83:1174–1178.

Wilden, U., and H. Kuhn. 1982. Light-dependent phosphorylation of rhodopsin: number of phosphorylation sites. *Biochemistry.* 21:3014–3022.

Wong, F. 1977. Mechanisms of the phototransduction process in invertebrate photoreceptors. PhD thesis. The Rockefeller University, New York.

Yamada, T., Y. Takeuchi, N. Komori, H. Kabayashi, Y. Sakai, Y. Hotta, and H. Matsumoto. 1990. A 40-Kilodalton phosphoprotein in the *Drosophila* photoreceptor is an arrestin analog. *Science.* 248:483–486.

Yeandle, S. 1958. Evidence of quantized slow potentials in the eye of *Limulus*. *American Journal of Ophthalmology.* 46:82–87.

Yeandle, S., and J. B. Spiegler. 1973. Light-evoked and spontaneous discrete waves in the ventral nerve photoreceptor of *Limulus*. *Journal of General Physiology.* 61:552–571.